

The mutated BRAF inhibitor vemurafenib and the TRAIL receptor agonist APG350 imply synergistic antitumor effects in melanoma

Anna Hesenet Rosness

NORWEGIAN UNIVERSITY OF LIFE SCIENCES
Department of Chemistry, Biotechnology and Food Sciences
Master Thesis 60 credits 2013



Abstract

Malignant melanoma is one of the most devastating cancer types with aggressive metastasizing abilities and the capability to develop therapy resistance. Until recently, effective therapeutic options have been non-existing, but in 2011/2012 the mutated BRAF inhibitor vemurafenib/Zelboraf® was approved by the FDA and EU, showing improved overall survival compared to existing therapy. Unfortunately, the effects of the drug are short-lived and new strategies to overcome resistance are under intense investigation.

In the present work, combination therapy with vemurafenib and the TRAIL receptor agonist APG350 has been evaluated in 2D- and 3D-cultures of the melanoma cell lines Melmet 1 and Melmet 5. It was observed that combination of the two drugs induces synergistic effects compared to mono-therapy in both cell lines, but synergy was dependent on the culturing type and drug dose utilized. In Melmet 5, synergistic results were obtained in 2D-cultures, 3D-cultures and the PuMA-assay, although the latter was not fully optimized at the time of study and the results are therefore not conclusive. In Melmet 1, most of the concentrations tested in 2D-cultures indicated antagonistic effects, while synergy was obtained in 3D cultures using the same concentrations. Western analysis of both cell lines showed increased cleavage of caspase-9, caspase-3 and PARP as well as upregulation of Bim and downregulation of Mcl-1, suggesting enhanced activation of apoptotic pathways.

The melanoma cells' disposition for metastasizing and therapy resistance do not solely arise from intrinsic properties of the cell but are linked to tumor interactions with the microenvironment (TME), e.g. stromal cells, soluble molecules and extracellular matrix components. Thus components of TME should be taken into account when screening for new therapies, and conditioned medium from WI-38 lung fibroblasts and co-cultures were used to evaluate the impact of TME-effects on drug response. WI-38 cells affected the melanoma cells response to therapy by inducing decreased effect of vemurafenib and increased effect of APG350. The results also indicated that fibroblast secreted factors for the most part were responsible for the change in drug effect, but that direct cell-cell contact can contribute to change these effects.

Overall the results imply that combination therapy of APG350 and vemurafenib may be effective as a new therapeutic strategy for melanoma patients, but further studies on TME effects and validation of the results in additional cell lines and in *in vivo* models are needed.

Sammendrag

Malignt melanom er en av de mest alvorlige krefttypene med aggressive metastaserende egenskaper og med evne til å utvikle resistens mot terapi. Inntil nylig har effektive legemidler mot sykdommen vært ikke-eksisterende, men i 2011/2012 ble vemurafenib/Zelboraf®, en mutert BRAF-inhibitor som viser økt total overlevelse sammenlignet med eksisterende behandling, godkjent av både FDA og EU. Dessverre er effekten av legemiddelet kortvarig, og nye strategier for å overkomme resistens er under intens forskning.

I det gjeldende arbeidet har kombinasjonsbehandling med legemiddelet vemurafenib og TRAIL-reseptor agonisten APG350 blitt evaluert i 2D- og 3D-kulturer med melanom cellelinjene Melmet 1 og Melmet 5. Det ble observert at kombinasjon av de to medikamentene gir synergistiske effekter i forhold til monoterapi i begge cellelinjer, men synergi var avhengig av dyrkningsformen og medikamentdose. I Melmet 5 ble synergistiske resultater oppnådd ved bruk av 2D-kulturer, 3D-kulturer og PuMA, men sistenevnte var ikke fullt ut optimalisert ved undersøkelsestidspunktet og er derfor ikke konkluderende. I Melmet 1 ga de fleste testede medikamentkonsentrasjonene antagonistiske effekter i 2D-kulturer, mens 3D-kulturer viste synergi med de samme konsentrasjonene. Western analyser av begge cellelinjer viste økt kløyving av caspase-9, caspase-3 og PARP, i tillegg til oppregulering av Bim og nedregulering av Mcl-1, noe som tyder på økt aktivering av apoptotiske signalveier.

Melanomcellers evne til metastasering og utvikling av terapiresistens oppstår ikke kun utifra indre egenskaper hos cellene, men er knyttet til interaksjoner med tumor mikromiljøet (TME) gjennom f.eks. stromale celler, løselige molekyler og ekstracellulære matriks-komponenter. Dermed bør man ta hensyn til TME ved screening av nye virkestoffer, og kondisjonert medium fra WI-38 lungefibroblaster og ko-kulturer ble brukt til å evaluere effekten av TME på medikamentrespons. WI-38 celler påvirket melanomcellenes terapirespons ved å gi redusert virkning av vemurafenib og økt virkning av APG350. Resultatene antyder i tillegg at faktorer sektrert av fibroblaster hovedsakelig var ansvarlig for endringen i medikamenteffekt, men at direkte celle-cellekontakt kan bidra til å forandre disse effektene.

Alt i alt antyder resultatene at kombinasjonsbehandling med APG350 og vemurafenib kan være effektiv som en ny terapeutisk strategi for melanom pasienter, men flere studier på TME-effekter og validering av resultatene i flere cellelinjer og i *in vivo*-modeller er nødvendig.

Acknowledgments

The present work was performed at the Department of Tumor Biology, Institute for Cancer Research, The Norwegian Radium Hospital, Oslo University Hospital in collaboration with the Norwegian University of Life Sciences in the period August 2012 to May 2013.

First of all, I would like to thank my main supervisor Birgit Engesæter whose guidance and support has been essential for the completion of this thesis. I have especially valued our day to day collaboration and how you have always taken time to answer my questions and help me get back on track, even in stressful times. Your constructive and critical comments throughout the writing process has helped develop my understanding of academic writing and contributed to evolving the thesis into what it is today. Additionally, your knowledge, pedagogic skills and patience has made this year interesting and inspiring, and your constant support has helped me keep my head cool and aimed for the goal.

I also want to express my gratitude to the leader of the group, Gunhild M. Mælandsmo, for giving me the opportunity to work on this project and for taking the time to give feedback and objective comments throughout the project. Lina Prasmickaite, Kotryna Vasiliauskaitė, Ingrid Bettum, Karianne Fleten and Solveig Pettersen – your help has been invaluable. To the master students of the “master-room” providing a great working environment and all the other group members who has provided inputs and showed their support – thank you! I am also grateful to my supervisor at UMB, Tor Lea, for his help with practical issues regarding the completion of the thesis.

Additionally, I must include a separate section reserved for thanking my fantastic personal support team who has kept cheering me on – my dedicated dad, encouraging mom and inspiring sister. Your advice and moral support through 20 years (!!) of education has given me the foundation I’ve needed to get to where I am today.

And finally, last but not least, to my loving and patient Håvar. You made it all worthwhile.

Anna Hesenet Rosness

Mai 2013, Oslo

Table of Contents

Abstract	1
Sammendrag	3
Acknowledgments	5
Table of Contents.....	7
List of abbreviations	11
1. Introduction	13
1.1 Malignant melanoma.....	13
1.1.1 BRAF mutations in melanoma	14
1.1.2 Therapy for malignant melanoma.....	15
1.1.2.1 The mutated BRAF inhibitor vemurafenib.....	16
1.1.3 Influence of the tumor microenvironment (TME).....	17
1.1.3.1 Two-dimensional vs. three-dimensional cultures	19
1.2 Apoptosis.....	19
1.2.1 Caspases and Inhibitors of Apoptosis (IAPs)	20
1.2.2 The Bcl-2 family of proteins	22
1.2.3 TRAIL induced apoptosis.....	22
1.2.3.1 The TRAIL receptor agonist APG350	23
1.3 Other types of cellular death	24
Aims of the study	26
2. Materials and Methods	27
2.1 Cell lines	27
2.1.1 Melmet cells	27
2.1.2 WI-38 lung fibroblasts.....	28
2.2 General cell work.....	29
2.2.1 Cell culturing and sub-culturing.....	29
2.2.2 APG350 and vemurafenib	29
2.3 2D-experiments.....	30
2.3.1 Monocultures.....	30
2.3.2 Co-cultures	30
2.3.3 Treatment of 2D-cultures.....	30
2.3.3.1 Mono-therapy and combination therapy with vemurafenib and APG350.....	31
2.3.3.2 Conditioned medium infused with vemurafenib and APG350.....	31
2.3.4 CalcuSyn analysis.....	32
2.4 3D-experiments.....	32

2.4.1 Seeding of spheroids.....	32
2.4.2 Treatment of spheroids	32
2.4.3 Phase contrast imaging and measurement of spheroid radius	33
2.5 Cell Viability	33
2.5.1 CellTiter 96® AQueous One Solution Cell Proliferation Assay (MTS-assay).....	33
2.5.2 CellTiter-Glo® Luminescent Cell Viability-assay	33
2.5.3 Luciferase-assay	34
2.6 Western Immunoblotting.....	34
2.6.1 Culturing, treatment and harvesting of cells for Western Immunoblotting	35
2.6.2 Protein lysates.....	36
2.6.3 Measurement of protein concentration	36
2.6.4 NuPAGE® Bis-Tris Electrophoresis System.....	36
2.6.5 Blotting.....	37
2.6.6 Immunodetection.....	38
2.7 PuMA-assay	39
2.7.1 Phase contrast and fluorescent imaging, quantification of fluorescence intensity and immunohistochemistry staining.....	41
3. Results	42
3.1 The sensitivity of Melmet cells to vemurafenib and APG350	42
3.1.1 Mono-therapy in 2D-cultures	42
3.1.2 Combination therapy in 2D-cultures	43
3.1.3 Mono-therapy and combination therapy in 3D-cultures.....	45
3.2 Protein expression in Melmet cells treated with vemurafenib and APG350.....	48
3.3 Evaluation of lung fibroblasts impact on Melmet cells exposed to vemurafenib and APG350..	51
3.4 Evaluation of mono-therapy and combination therapy in mouse lung tissue	53
4. Discussion	57
Future perspectives.....	63
References	64
Appendix	69
I) List of reagents and materials.....	69
II) Details related to the Calcsyn data program.....	71
III) Example of spheroid volume calculations	71
IV) Luciferin solution	71
V) Lysis buffer	72
VI) Example of protein concentration and protein volume calculations.....	72
VII) R&D-buffer, pH 7,5	74

VIII) Stripping solution.....	74
IX) PuMA-medium.....	74
X) Supplementary data.....	75

List of abbreviations

BCA	Bicinchoninic acid
Cyt-c	Cytochrome-c
DcR	Decoy receptor
DR	Death receptor
DTIC	Dacarbazine
ECM	Extracellular matrix
EGF	Epidermal growth factor
FCS	Fetal calf serum
FGF	Fibroblast growth factor
FDA	US Food and Drug Administration
GFP	Green fluorescent protein
HGF	Hepatocyte growth factor
HD IL-2	High dose interleukin 2
IAP	Inhibitor of apoptosis protein
IHC	Immunohistochemistry staining
HGF	Hepatocyte growth factor
HRP	Horse radish peroxidase
LDS	Lithium Dodecyl Sulphate
Luc	Luciferase
MAPK	Mitogen Activated Protein Kinase
MMPs	Matrix metalloproteinases
OS	Median overall survival
PFS	Progression free survival
PLX	Vemurafenib
PuMA	Pulmonary Metastasis Assay
ROS	Reactive oxygen species
SD	Standard deviation
SDS	Sodium Dodecyl Sulfate
SEM	Standard error of the mean
TME	Tumor micro environment
TNF	Tumor necrosis factor
TRAIL	Tumor necrosis factor Related Apoptosis Inducing Ligand

1. Introduction

1.1 Malignant melanoma

Malignant melanoma of the skin is considered to be one of the most aggressive types of all human cancers and is the most deadly type of skin cancer¹. The Cancer Registry of Norway states that malignant melanoma was one of two cancer types with the strongest increase in incident rates in Norway in 2010, with 1518 new incidents². The number of deaths was 338², making the top 10 list of cancer types with the highest death rate in Norway. In addition to this, malignant melanoma affects young people in a larger scale than most other solid tumor cancers, thereby giving a dramatic effect in terms of years lost.

Malignant melanoma originates in melanocytes, the pigment producing cells predominantly found in the skin³. Melanocytes are derived from neural crest cells and are found along the basement membrane in the basal layer of the epidermis⁴. The cells produce the dark pigment melanin which absorbs UV-light and thereby protects the dermis from UV-radiation^{5, 6}. The transformation of melanocytes to tumor cells is a process not altogether understood but is known to involve, among other things, genetic sequential alterations, activation of oncogenes, inactivation of tumor suppressor genes and impaired DNA-repair⁴. These may occur due to environmental factors; exposure to UV-radiation being especially emphasized as a central part in the pathogenesis of the disease⁵. UV-radiation causes genetic changes, impairs immune function and induces formation of reactive oxygen species (ROS) which is DNA damaging⁶. Over-exposure to sunlight and/or sunbed tanning can therefore dramatically increase the risk of developing malignant melanoma⁷. The risk is also higher for people with fair skin, families with a history of melanoma, people with multiple benign or atypical nevi and latitude of residence for Caucasian people^{5, 6}.

The classic melanoma progression from a benign nevus to metastasizing tumor cells is shown in figure 1.1. See chapter 1.1.3 for more information about malignant melanomas ability to metastasize.

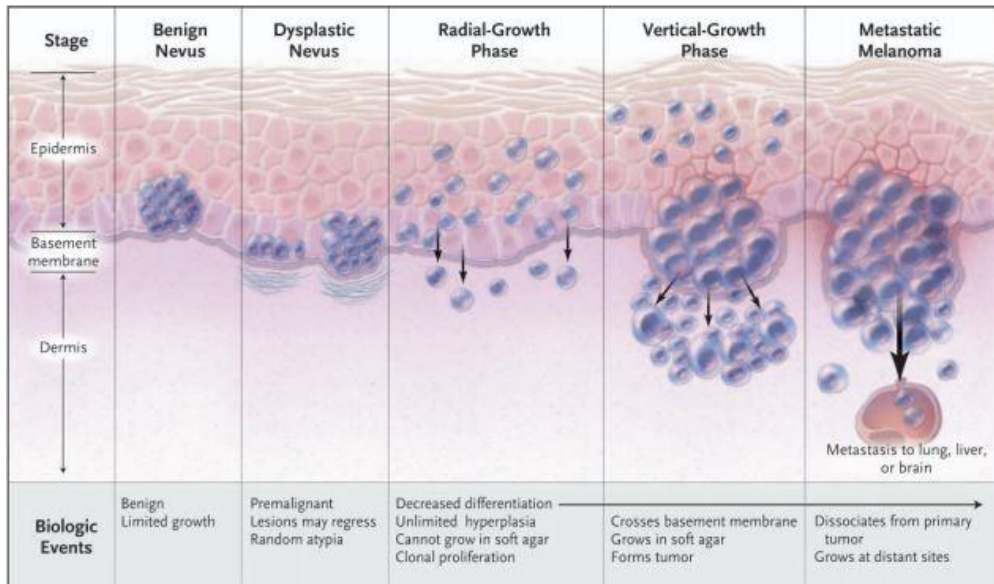


Figure 1.1: A model of the development and progression of malignant melanoma through several steps. **1:** Benign nevi are common in the overall population and are restricted to the basal layer of the epidermis. **2:** If the nevus develops an atypical structure and architecture the nevus may be premalignant and progress to the radial growth phase or it may regress. **3:** The malignantly transformed melanocytes proliferate radially, but don't have the ability to metastasize. **4:** In the vertical growth phase the melanocytes break through the basement membrane and invade the dermis. **5:** Metastatic melanoma, where the cells dissociate from the primary tumor and spreads to secondary sites. The picture is adapted from Miller and Mihm, 2006⁶.

The prognosis of malignant melanoma is strongly related to the stage at which it is detected. Patients diagnosed with primary cutaneous melanoma at an early stage can be treated with surgery and the overall survival is high, with a five year survival of 90 %⁸. However, when the cancer has metastasized to other parts of the body, usually the lung, liver or brain, it shows a much more aggressive phenotype and the survival rates fall dramatically with a median survival of 6 months and a five year survival of only 5-22 %⁸. The low survival rates are due to the resistance of most metastasized tumors to chemotherapy and radiotherapy, leaving few therapeutic options for advanced stages^{3, 9}. Early detection of the disease is therefore crucial for a good prognosis. Recently new drugs showing effect on overall survival have been approved in Europe and USA, as described in chapter 1.1.2.

1.1.1 BRAF mutations in melanoma

B-Raf is one of three functional Raf proteins in humans along with A-Raf and C-Raf. The Raf proteins are serine threonine kinases that play a role in the regulation of the mitogen-activated protein kinase signaling pathway (MAPK-pathway)⁹. The activation of the pathway is initiated by RAS-GTP binding and the resulting RAF/MEK/ERK cascade leads to regulation of cell growth, proliferation and differentiation in response to growth factors, cytokines and hormones¹⁰. Activated RAS can promote dimerization of B-Raf and C-Raf, the cooperation leading to full activation of ERK^{11, 12}. Figure 1.2 shows a simplified version of the MAPK pathway.

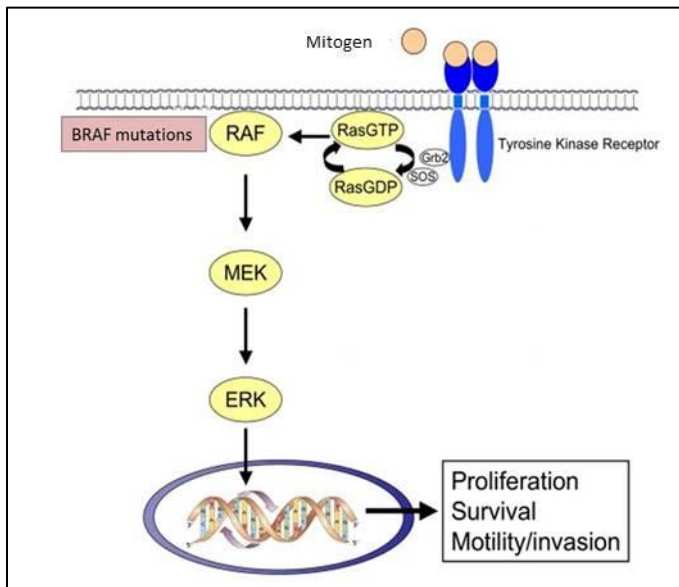


Figure 1.2: A schematic presentation of the MAPK-pathway. Receptor Tyrosine Kinases (RTKs) are activated by mitogen binding to the extracellular domain of the receptor. This activation leads to Ras-GTP binding and the transferring of signals through the pathway by phosphorylation of RAF, MEK and ERK. ERK modulates gene expression through the regulation of transcription factors promoting cell proliferation and survival. The figure is adapted and modified from Montagut & Settleman 2009¹³.

B-Raf is the most frequently mutated protein kinase in human cancers and is found in over 50% of all melanomas^{14, 15}. The most common BRAF gene mutation, accounting for more than 80 %⁹, is a substitution of valine to glutamic acid at position 600 (V600E), which can result in a 500-fold overactivation of the B-Raf kinase activity¹⁰. Also V600K and V600D are common, seen in 16 % and 3 % of all BRAF mutations⁹. An overactive BRAF gene will lead to an overactive signaling cascade through the MAPK pathway, resulting in excessive cell proliferation. Also, the overactive cascade increases melanoma cell survival by regulating the expression of several pro-apoptotic and anti-apoptotic proteins like Bim, Bad and Mcl-1^{9, 16}.

Inhibition of mutated BRAF has been a focus area in melanoma research since 2002⁹ and seems to be a strategy with quite large impact, leading to e.g. the development of the drug vemurafenib.

1.1.2 Therapy for malignant melanoma

Until 2011, only two drugs were approved by the US Food and Drug Administration (FDA) as therapy for metastatic melanoma; the anti-neoplastic chemotherapy agent dacarbazine (DTIC) and the immune-modulating high dose interleukin 2 (HD IL-2)¹⁷. Neither of these drugs increases median overall survival and they both have a low response rate. Also HD IL-2 is a highly toxic agent associated with severe side effects^{17, 18}. In addition to these therapies, high dose interferon alfa-2b is approved for adjuvant therapy of resected high-risk melanoma¹⁹. In Norway only DTIC and interferon alfa-2b, not HD IL-2, has been approved for use.

Many experimental drugs have been tested in clinical trials the last 20 years with the hope of improving the prognosis of metastatic melanoma, but there has not been much progress until recently.

In 2011 the FDA approved two novel drugs; the immune stimulatory agent ipilimumab and the BRAF V600E inhibitor vemurafenib. These drugs represent a huge leap in melanoma therapy and are a result of our time's increased understanding of melanoma biology, molecular characteristics and tumor immunology. Even though the drugs give a better overall survival than previous drugs and for the most part give more manageable toxicities, both therapies have their limitations and continued research is necessary to improve their effect.

1.1.2.1 The mutated BRAF inhibitor vemurafenib

Vemurafenib, a small molecule inhibitor of the BRAF V600E mutation, gets its name from **V600E mutated BRAF** inhibition and is also known under the name PLX 4032 and Zelboraf®. The drug is developed by Plexxikon Inc. and Hoffmann-La Roche for the treatment of late-stage melanoma. The drug was in 2011 approved by the FDA and in 2012 also by Health Canada and the European Commission²⁰.

Vemurafenib is specific against mutant BRAF V600E and V600K. It selectively binds BRAF-monomers and inhibits their activity, thereby preventing phosphorylation of MEK and ERK i.e. inhibiting activation of the MAPK pathway. An indirect apoptotic response with increased Bim expression, downregulation of Mcl-1 and dephosphorylation of Bad has also been observed with MEK and ERK inhibitors^{9, 16, 21}. The response in patients with the selected mutations has been very convincing. The phase I clinical trial showed significant tumor regression in 81 % of the BRAF^{V600E} metastatic melanoma patients¹⁸. The 1-year survival was shown to be ~50 % and the 2-year survival to be 38 % with a median overall survival (OS) of 13,8 months⁹. The phase II trial (BRIM-2) showed a 52 % response rate and progression free survival (PFS) of 6,2 months¹⁷. The phase III trial (BRIM-3) was a randomized trial where metastatic melanoma patients were treated with either vemurafenib or dacarbazine. A clear OS benefit was seen in vemurafenib vs. dacarbazine, with a response rate of 48 % vs. 5 % and PFS of 5,3 months vs. 1,6 months. Also 84 % vs. 64 % of the patients were alive after 6 months^{9, 17}.

Despite the good results reported in the clinical trials, the responses to vemurafenib are typically short-lived with relapse occurring in almost every case. This suggests the existence of intrinsic BRAF inhibitor resistance, something that has been documented in preclinical studies⁹. One resistance mechanism recently discovered is a 61-kDa splicing variant of BRAF V600E which lacks the exons that encompass the RAS-binding domain¹¹. BRAF lacking this domain are able to dimerize independently of RAS signaling, giving a BRAF V600E variant that is resistant to vemurafenib²². Acquired resistance after initial response to the drug is also well documented e.g. through gain in BRAF V600E copy number, through acute increase in C-Raf and through activating mutations in

NRAS^{23, 24}. Additionally, resistance can be achieved through activation of the PI3K-AKT and RAS-C-Raf-MEK pathways.

Different strategies to overcome resistance have been proposed, for example Thakur et al. (2013)²⁵ has shown that drug-resistant cells may display drug dependency, and exploits this by proposing a treatment strategy which involves giving pulses of vemurafenib instead of continual treatment. The study reveals that intermittent dosing exploits the fitness deficit seen in drug dependent tumor cells in the absence of the drug, and the cells remain responsive to vemurafenib²⁵. Another way to overcome resistance is combination therapy, a long used strategy that has become even more appealing with the development of new targeted drugs. The aim is to target several driver mutations in the tumor simultaneously. It has been shown that tumor responses in vemurafenib-treated patients are very sensitive to small changes in pathway inhibition¹⁴, therefore one can assume that knocking out several pathways simultaneously may lead to a greater chance of effect. Also, combination with a drug targeted toward the same pathway may prove to be more efficient than vemurafenib alone. For instance, combination with drugs targeted towards the PI3K-AKT pathway or inhibitors of MEK can be efficient in delaying or preventing relapse²³. In addition to these benefits, combination therapy could allow drug doses to be lowered, possibly leading to a reduction of side effects. But when combining two drugs there is always the possibility that new side-effects develop, which may cause worse symptoms than the original mono-therapy. Therefore extensive testing is necessary to be sure the combination is safe.

To sum up, the clinical trials of vemurafenib show convincing high response rates and low toxicity, but they also reveal less optimistic results showing a relatively short duration of drug effect and a high relapse rate. Paradoxically, vemurafenib has also shown an adverse effect on cells with non-mutated (wild-type) BRAF²⁶. In wild type cells the drug activates RAF and enhances ERK signaling leading to increased proliferation in primary melanoma and increased motility in metastatic melanoma²¹. Ongoing research is therefore necessary to improve the drugs effect and response-duration, and efforts should be made to tailor treatments to specific genetic compositions of the tumor.

1.1.3 Influence of the tumor microenvironment (TME)

One of the hallmarks of malignant melanoma is its high ability to metastasize. This way to invade other tissues is a complex process shortly summarized in figure 1.3. Where it earlier was thought that the cancer cells ability to metastasize was mostly an intrinsic property of the cell, it is now known that the tumor microenvironment plays an important role. Interestingly, this is not a new idea. The “seed and soil” hypothesis of Stephen Paget was presented over a century ago in 1889, and suggests that tumor cells (the seed) can colonize distant organs (the soil) only where there is a favorable

environment for tumor growth²⁷. This theory was however mostly ignored up until recently when TME has become a popular area of study. It is now known that tumors can contribute to shaping their own microenvironment and that the modifications that occur can support cell proliferation and metastasis.

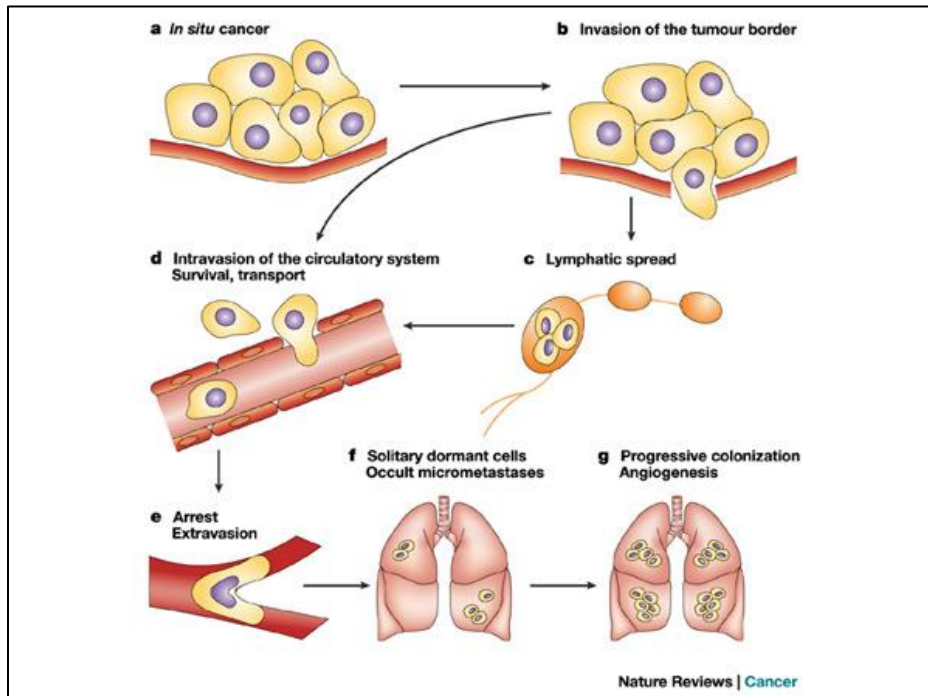


Figure 1.3: A schematic presentation summarizing the metastatic process. A) Tumor growth. B) Invasion through the endothelial basement membrane, requiring reversible changes in cell-cell and cell-matrix adhesion proteins. C) and D) Cells enter the blood and/or lymphatic system where they are transported to secondary sites. The cells have to survive in the blood by i.e. avoiding immune recognition. E) Surviving cells can become arrested in capillaries of distant organs where they must adhere to the endothelia and extravasate into the tissue. F) Metastatic colonization of the secondary site progress through single cells to micrometastasis. Cells can lay dormant for many years before this progression. G) Progressively growing tumors and development of a vascular network; angiogenic metastases. Adapted from Steeg 2003²⁸.

The TME consists of supporting connective tissue, the stroma, providing a framework for the tumor²⁹. The stroma is built up of non-malignant cells like fibroblasts, endothelial cells, smooth muscle cells and bone marrow-derived cells including macrophages and immune cells. These cells can secrete a variety of inflammatory-, growth- and survival-factors like cytokines and chemokines, as well as extracellular proteases and pro-inflammatory molecules, all of which can enhance a tumors ability for survival, growth and invasion throughout the different steps of the metastatic cascade³⁰ (figure 1.3). In mammalian tissue a structure called the extracellular matrix (ECM) is also prominent in the cells network. The ECM contains among other things collagen, elastin and laminin which give the tissue its mechanical properties as well as help organize communication between the cells³¹.

The TME not only plays an important role in cancer progression and metastasis, but also in regard to drug response. A recent study by Straussman et al.(2012) shows that “anticancer drugs capable of

killing tumor cells are rendered ineffective when tumor cells are cultured in the presence of stromal cells³². These findings propose that drug resistance may be caused or partly caused by factors secreted by the TME. The same study also identifies HGF as a factor correlated with innate (immediate) RAF-inhibitor resistance. HGF induces activation of the receptor tyrosine kinase MET, which is reported to be overexpressed in melanoma³². According to Staussman's study "HGF can induce sustained activation of both ERK and AKT (...) predicting that both the MAPK pathway and the PI3K-AKT pathway contribute to the primary resistance induced by HGF-secreting stromal cells³². By combining vemurafenib with a c-MET inhibitor one may be able to overcome resistance.

1.1.3.1 Two-dimensional vs. three-dimensional cultures

In experimental cell culturing two-dimensional (2D) cultures are commonly used as an initial approach to drug screens due to the simplicity of the assays. In 2D-cultures the cells will have approximately 50 % of their surface area exposed to hard plastic and have minimal cell-cell and cell-ECM interactions, which is not comparable to how cells grow *in vivo*. The 2D-cultures therefore have significant limitations in regard to reproducing the complexity and pathophysiology of tumor tissue³³. Three-dimensional (3D) cultures have proved to be better mimics of how cells grow *in vivo*, better reflecting the TME and cell-cell interactions³⁴. Several 3D-culture systems exist, e.g. whole perfused organs, tissue explants and gel/matrix-based cultures, but multicellular tumor spheroids are, according to Vinci et.al. (2012), best characterized and most widely used³³.

1.2 Apoptosis

Apoptosis is a highly selective and tightly regulated form of programmed cell death. The term is described by Wong (2011) as a situation where "a cell actively pursues a course toward death upon receiving certain stimuli"³⁵. The cellular suicide is characterized by cell shrinkage and chromatin condensation as well as nuclear fragmentation and cytoskeleton degradation with loss of membrane integrity^{35, 36}. Recognition by phagocytic cells before loss of membrane integrity makes apoptosis immunologically silent³⁷.

Apoptosis plays an important role in fetal and embryonic development, e.g. in the sculpting of tissue, and in adult multicellular organisms where it contributes to tissue remodeling and control of cell number and is crucial in the maintenance of homeostasis³⁵⁻³⁹. But apoptosis is also seen in cells exposed to stressful stimuli and cells that have undergone harmful damage. Deregulation of apoptosis can lead to various pathologies. The reduced ability to induce apoptosis is linked to uncontrolled cell growth, carcinogenesis and autoimmune diseases³⁷. Excessive or inappropriate apoptosis contributes to injuries accompanying diseases like Alzheimer's and stroke³⁹. Targeting different aspects of apoptosis is emerging as an important strategy for treatment of cancer^{35, 39}.

1.2.1 Caspases and Inhibitors of Apoptosis (IAPs)

Apoptosis is mainly regulated through two different pathways, the extrinsic and intrinsic pathway, both involving cysteine proteases called caspases³⁵. Caspases are the central players in apoptosis, cleaving several vital proteins in the cytoskeleton and nuclear scaffold^{35, 39}. Caspases are synthesized as inactive monomers, procaspases, and are typically activated by oligomerization following proteolytic cleavage by other active caspases or autoproteolysis^{36, 37}. Initiator caspases (caspase-2, -8, -9, -10) are found at the start of the proteolytic cascade and activate downstream executioner procaspases (caspase-3, -6, -7) which again cleave target proteins in the cell. Different cell types can be classified as type I and type II cells based on the intrinsic pathways activation status. Type I cells activate caspase-3 without involvement of the intrinsic pathway, while type II cells activate both the extrinsic and intrinsic pathways through cleavage of Bid, leading to an amplification of the caspase cascade⁴⁰. Figure 1.4 shows and describes the two main apoptotic pathways, both leading to caspase-3 activation.

Inhibitors of apoptosis are proteins with the ability to bind to and inhibit or degrade activated caspases³⁶. X-linked IAP (XIAP) seems to be one of the central players with regard to direct caspase-3 and 9 blocking⁴¹. The intermembrane mitochondrial protein Smac/DIABLO works as an anti-IAP, blocking IAPs in the cytosol, and in this way promotes apoptosis.

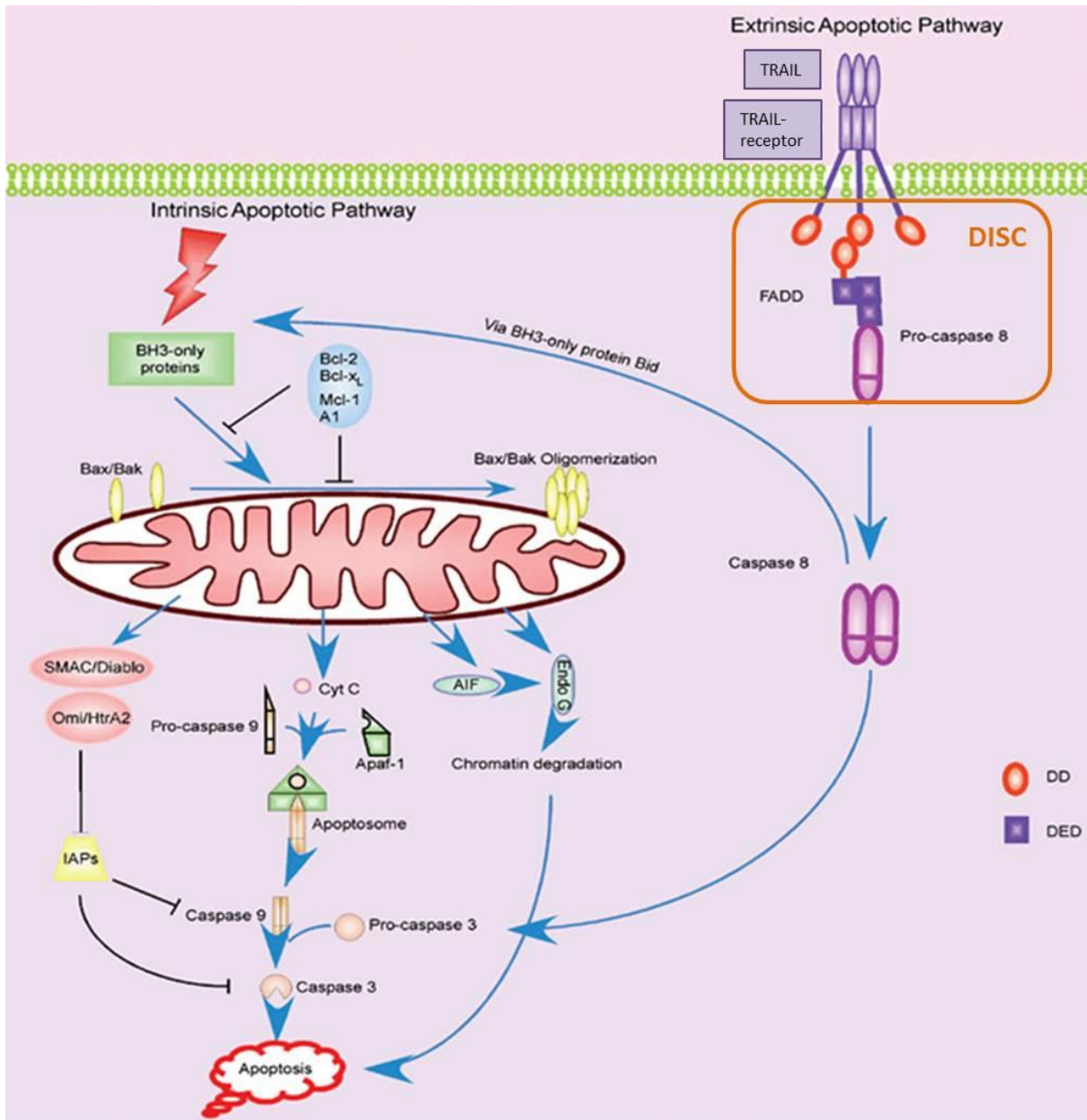


Figure 1.4: An overview of the intrinsic and the extrinsic pathway of apoptosis. The extrinsic pathway is activated by death ligands, like TRAIL (chapter 1.2.3) or FAS-ligand, binding to death receptors on the cell surface. An intracellular DISC complex is formed which includes the adaptor protein FADD and initiator procaspase-8 or 10³⁶. The DISC brings the procaspases into close proximity with each other so they can be activated. The active caspases cleave downstream procaspase-3 to active caspase-3. The intrinsic pathway is activated by a variety of stresses, like UV-radiation and DNA-damage³⁹. It can also be activated through the extrinsic pathway by cleavage of the BH3-only protein Bid to tBid. The pathway is the result of increased mitochondrial permeability due to Bax/Bak oligomerization forming pores that release pro-apoptotic molecules like cytochrome-c into the cytoplasm (chapter 1.2.2). Cyt-c associates with Apaf-1 and procaspase-9 to form the apoptosome. This is a complex that leads to the activation of procaspase-9, which further activates procaspase-3. Both pathways thereby lead to the activation of caspase-3 which results in apoptosis. The figure is modified from Zhang (2005)⁴².

1.2.2 The Bcl-2 family of proteins

The intrinsic pathway of apoptosis is tightly regulated by the Bcl-2 family of proteins³⁶. These proteins can be divided into three groups based on their effect on apoptosis; the anti-apoptotic Bcl-2 proteins, the pro-apoptotic Bcl-2 proteins and the pro-apoptotic BH3-only proteins, all of which will either promote or inhibit the release of cytochrome-c (cyt-c) and other intermembrane mitochondrial proteins into the cytosol. The balance between these proteins is more important for apoptosis induction than the absolute quantity³⁵.

The Bcl-2 family members are mainly located on the outer mitochondrial membrane. Anti-apoptotic proteins, like Bcl-2 itself and Mcl-1 inhibit apoptosis by binding to and inhibiting pro-apoptotic proteins like Bax and Bak. In times of cellular stress pro-apoptotic BH3-only proteins, like Bim, Bad and Bid, initiate apoptosis by binding to and neutralizing anti-apoptotic proteins. They thereby enable Bax and Bak to associate and form a pore, leading to increased mitochondrial permeability and release of cyt-c and other mitochondrial proteins into the cytosol³⁶. As described in figure 1.4, cyt-c is necessary in the formation of the apoptosome, a complex essential for procaspase 9 activation and apoptosis induction³⁵.

Bim is known to be the only BH3-only protein that can bind and inhibit all anti-apoptotic Bcl-2 family proteins, and in addition directly bind and activate Bax, thereby making it a potent apoptosis inducer⁴³. The pro-apoptotic protein Bad can be phosphorylated at three sites, serine 112, 136 and 155, leading to a change in the proteins function resulting in loss of the ability to bind and neutralize anti-apoptotic proteins. Phosphorylation of Bad at serine 112 requires activation of the MAPK-pathway, phosphorylation of serine 136 is in accordance with Akt-activation, and phosphorylation of serine 155 follows growth factor stimulation⁴⁴.

1.2.3 TRAIL induced apoptosis

TRAIL is the short term for Tumor necrosis factor Related Apoptosis Inducing Ligand. It is a protein member of the death receptor (DR) ligand family which is a subclass of the tumor necrosis factor (TNF) superfamily⁴⁵. TRAIL is a type II transmembrane protein normally expressed on the membrane of some types of immune cells, as well as human tissues found in e.g. the spleen, prostate and lung⁴⁶.

TRAIL can activate the extrinsic pathway of apoptosis (figure 1.4) by binding to and activating death receptors DR4 and DR5 by receptor trimerization (figure 1.5 A). These receptors contain functional, intracellular death domains and can transmit apoptotic signals into the cell. TRAIL can also bind two decoy receptors; DcR1 and DcR2, which either lack the death domain (DcR1) or contain a truncated death domain (DcR2), making them unable to activate the apoptotic pathway⁴⁵. Additionally, TRAIL

receptors can stimulate non-apoptotic signals like various protein kinase cascades leading to activation of e.g. ERK and the transcription factor NFκB, both promoting cell survival^{47, 48}.

Research indicates that TRAIL induces apoptosis mainly in cancer cells, but not in normal tissue^{46, 49}. This was early on postulated to be because normal cells mainly express the decoy receptors and are found to have lower amounts of death-receptors, making them unable to convey an apoptotic signal into the cell^{45, 49-51}. However, it has not been proven that the amount of DcR and functional DR correlate with TRAIL sensitivity in cancer cells⁴⁵. Even so, the specificity towards cancer cells gives TRAIL a huge potential as an anticancer agent. Unfortunately there are also challenges related to TRAIL, mainly in the form of TRAIL-resistance which can be both inherited and acquired⁴⁷. Because decoy receptors bind TRAIL with the same affinity as the death receptors, they can provoke resistance to TRAIL-mediated apoptosis by competing with DR4 and DR5^{46, 47, 50}. Complicating things more is the issue that approximately one third of melanoma cell lines show resistance to TRAIL even though they have high levels of death receptors on their surface⁴⁹. This can be explained in several ways, for example by loss of caspase-8, dysfunctional FADD or caspase-3 inhibition by XIAP^{48, 49}. Because of resistance issues it has become apparent that TRAIL agonists as mono-therapy are efficient for only a limited number of patients, and combined therapy could therefore be an approach to maximize the therapeutic effect of TRAIL⁴⁵.

Several clinical agents targeting TRAIL have been approved as drugs and even more are under clinical testing. Examples include recombinant TRAIL agents, anti-TRAIL receptor antibodies and gene therapy agents expressing TRAIL⁴⁷. Toxicity associated with such therapeutics is low, unlike most other anti-cancer drugs. However, studies have shown that tumor cells which are resistant to TRAIL-induced apoptosis may react to TRAIL treatment with increased growth and metastasis^{47, 48}. This could be explained by TRAILs ability to activate other signaling pathways, like the MAPK pathway or NFκB, alongside the apoptosis machinery⁴⁷. It is therefore of vital importance to identify patients with TRAIL resistant tumors before treatment with TRAIL receptor targeted drugs.

1.2.3.1 The TRAIL receptor agonist APG350

APG350 is a TRAIL receptor agonist developed by Apogenix (Heidelberg, Germany) for the treatment of solid tumors. The agent consists of two single chain TRAIL-receptor binding domains dimerized via the Fc-part of a human IgG molecule, creating six receptor binding sites per molecule (figure 1.5B). This enables the compound to bind to and induce trimerization of several TRAIL-receptors simultaneously, forming active TRAIL receptor multimers that activate apoptotic signaling. APG350 only binds to DR4 and DR5, not the decoy receptors. This ability to form multimers, along with it not requiring cross-linking via Fcα-receptors, distinguishes APG350 from other TRAIL receptor agonist, making it, according to the producer, more efficient in the induction of apoptosis⁵².

Clinical studies of APG350 will be initiated at the earliest in 2015, and the agent will most likely be developed in combination with already approved drugs or chemotherapeutics.

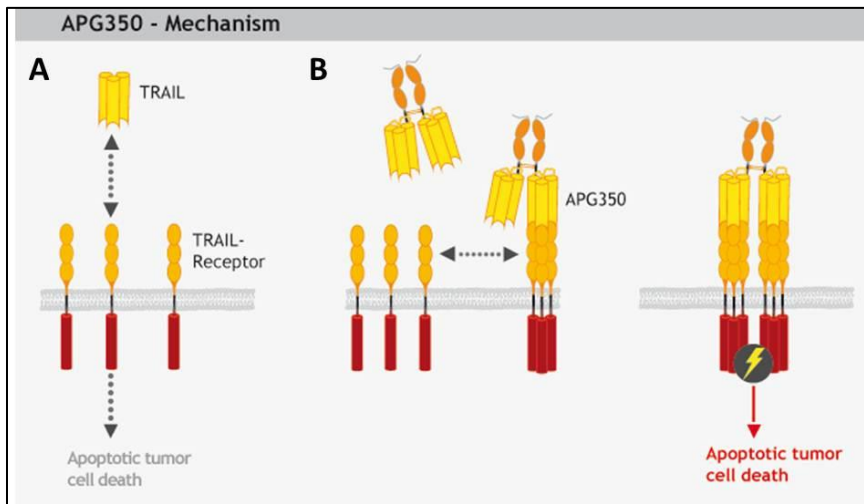


Figure 1.5: A) Illustration of how TRAIL in normal cells bind to TRAIL receptors on the cell surface and induce apoptosis by trimerization of the receptors. B) APG350 is a TRAIL receptor agonist that induces clustering of up to six TRAIL receptors simultaneously, forming highly active TRAIL receptor multimers. The figure is acquired from Apogenix.com

1.3 Other types of cellular death

The last decade it has become clear that apoptosis is not the only cell death program for removal of unwanted cells. Other types of cell death are autophagy, necrosis and pyroptosis. Necrosis is a form of cellular death associated with pathological conditions. Traditionally it was considered a passive and uncontrolled form of cell death resulting from physical damage, but it has lately become evident that in certain conditions necrosis can also be the result of regulated signaling. This caspase-independent cell death, often called necroptosis, can be activated by the same ligands as apoptosis. Thus they can act as a “back-up” cell death pathway in cells where caspase activation is hampered³⁷. In other words necrosis can act as a substitute for apoptosis. In contrast to apoptosis, necrosis will initiate an inflammatory response and affect neighboring cells³⁹.

Autophagy is a catabolic pathway that degrades and recycles dysfunctional or unnecessary cellular components through the lysosomal machinery, e.g. under times of cellular stress. Autophagy is well-established as a pro-survival role ensuring intracellular homeostasis, but autophagic activity may also accompany and in some cases lead to cell death³⁷. Several connections between autophagy and apoptosis and necrosis exists, and it is debatable whether autophagy is a distinct form of cell death or if it accompanies or triggers another form of cell death^{37, 53}.

Pyroptosis is a recently recognized form of cell death distinct from necrosis and apoptosis. It is seen in cells like macrophages, monocytes and dendritic cells infected with microbial pathogens and is part of the host defense system³⁷. Pyroptosis is dependent on caspase-1, a member of the inflammatory caspases not involved in apoptosis. It is activated in a complex called the inflammasome, an analogy to the apoptosome, and active caspase-1 induces pore formation in the plasma membrane leading to water influx, cell swelling and finally cell lysis⁵⁴. Caspase-1 activation leads to an inflammatory response.

Aims of the study

The aim of the present project was to evaluate the effect of combination treatment vs. mono-therapy with the mutated BRAF inhibitor vemurafenib and the TRAIL receptor agonist APG350 on malignant melanoma cells. Additionally, the impact of tumor microenvironment (TME) interactions on the therapy response was investigated with the lung as a model organ and fibroblasts as model cells.

Specific aims:

- 1) Evaluate the effect of combination therapy with vemurafenib and APG350 compared to mono-therapy on the cell lines Melmet 1 and Melmet 5 in 2D- and 3D-cultures.
- 2) Study the expression of apoptotic proteins after treatment with the antitumor drugs through Western immunoblotting analysis.
- 3) Study the impact of the TME on melanoma cells' response to the antitumor drugs through co-culture experiments, conditioned medium experiments and the PuMA-assay.

Through these investigations we anticipate to obtain valuable information regarding the impact of the TME on drug response in melanoma cell lines and to get an evaluation of the treatment potential of combining vemurafenib with APG350.

2. Materials and Methods

In this project Melmet cells were grown in both 2D- and 3D-cultures and treated with vemurafenib and/or APG350 to evaluate the cell lines' general drug response. Additionally, cells were cultured in conditioned medium, as co-cultures and in mouse lung tissue. The cells were analyzed with various assays to determine the cell viability, and Western immunoblotting was performed to evaluate protein expression. Figure 2.1 gives an overview of treatment strategies and methods of analysis for the various model systems. Additional information regarding the various setups can be found throughout this chapter. A list of reagents and materials used in the experiments are given in Appendix I.

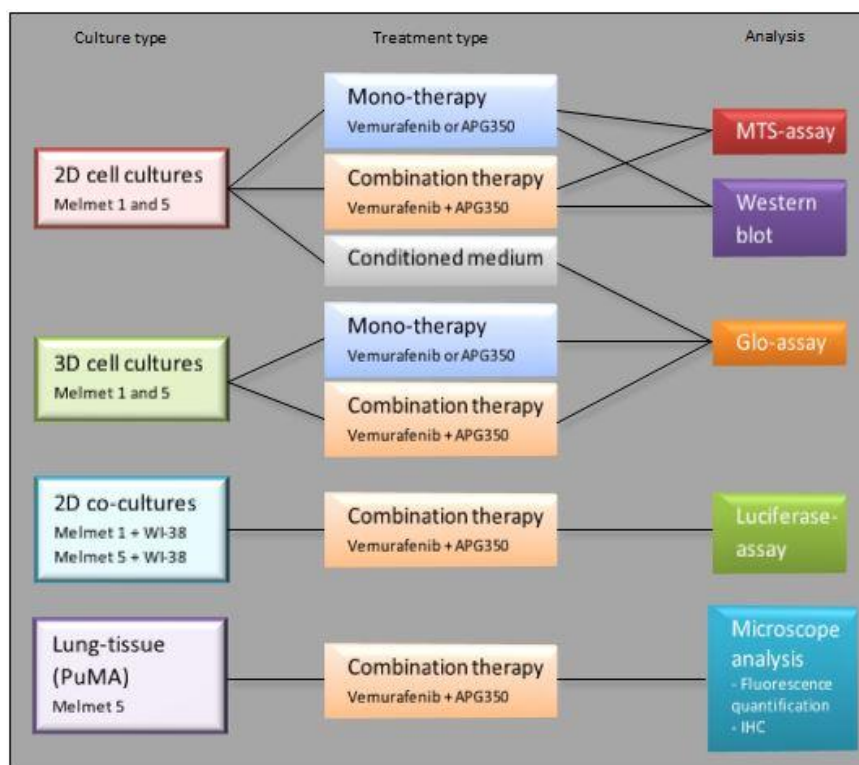


Figure 2.1: An overview of the different culture types, therapy treatments and assays used in this project.

2.1 Cell lines

2.1.1 Melmet cells

Two melanoma cell lines were used in this study, Melmet 1 and Melmet 5. The Melmet cells represent “close-to-patient” early-passage materials and are therefore proposed to be less differentiated than commercially available cell lines that have been cultured *in vitro*⁵⁵. The cell lines were established at the Norwegian Radium Hospital, Department of Tumor Biology, by isolation of cells from metastatic melanoma patient biopsies. The procedure was performed using immunomagnetic beads conjugated

with melanoma-specific antibody as described by Prasmickaite et al.⁵⁶. Table 2.1 gives an overview of background information regarding the cell lines.

Table 2.1: Information regarding the Melmet 1 and 5 cell lines.

	Melmet 1	Melmet 5
Source	36 year old female	56 year old male
Tissue (site of biopsies)	Subcutaneous	Lymph node
Common sites of metastasis	Preference to brain	Multiple sites: Brain, lung, liver, spinal cord ++
Phenotype	Invasive Low- proliferative	Proliferative Low-invasive
BRAF-V600E mutation	Yes	Yes
Tumorigenic ability in mice	Yes	Yes
Metastatic ability in mice	Yes	Yes

In the co-culture experiments (chapter 2.3.2) and in the PuMA assay (chapter 2.7) Melmet cells transfected with lentiviral vectors expressing GFP-luc were used. GFP is short for green fluorescent protein and luc is short for luciferase, an oxidative enzyme catalyzing the oxidation of luciferin to oxyluciferin which emits light (figure 2.3). These tags enable us to detect and distinguish Melmet cells from other cell types in the PuMA and co-culture assays. The lentiviral vector was a kind gift from Dr. Glenn Merlino (Laboratory of Cancer Biology & Genetics, National Cancer Institute, USA)⁵⁷, and the transfection was performed by Lina Prasmickaite (Department of Tumor Biology, Norwegian Radium Hospital).

All Melmet cells were cultured with RPMI 1640 medium supplemented with 10 % fetal calf serum (FCS) and 1 % GlutaMAX™, hereby referred to as RPMI+. See table 2.2 for an overview over all media used in the present study.

2.1.2 WI-38 lung fibroblasts

The lung fibroblasts WI-38 (#CCL-75) were bought from Americas Type Culture Collection (ATCC). The cell line was derived from normal embryonic lung tissue from a Caucasian female. The cells were stored in liquid nitrogen. Before use the cells were thawed and transferred to T75-flasks where they were cultured in EMEM medium with 10 % FCS.

Table 2.2: Medium types used in the culturing of different cell lines. Supplements to the original medium are also stated.

Cell lines	Medium	Supplements
Melmet 1	RPMI 1640	10 % fetal calf serum (FCS) 1 % GlutaMAX™
Melmet 5	RPMI 1640	10 % FCS 1 % GlutaMAX™
WI-38	EMEM	10 % FCS
Melmet 1 or 5 + WI-38 (co-cultures)	EMEM	10 % FCS

2.2 General cell work

2.2.1 Cell culturing and sub-culturing

Cells were cultured as monolayers in flasks with indicated medium (table 2.2). All cells were grown in an antibiotic free environment at 37°C in a 5 % CO² atmosphere, hereby referred to as “normal culturing conditions”. The cell cultures were inspected with an Olympus CKX41SF microscope and they were routinely split once or twice a week depending on the cell type. All cell procedures were performed under sterile conditions and the cells were tested regularly for mycoplasma infection.

Detachment of cells from cell flasks was done by adding EDTA or trypsin. The cell concentration was decided using the Countess™-automated cell counter. Cells were stained with 0,4 % Trypan Blue before counting to distinguish between live and dead cells. Only cells with compromised cell membranes, dead cells, will absorb Trypan Blue.

2.2.2 APG350 and vemurafenib

APG350 (Apogenix) was dissolved in PBS from the manufacturer to a stock concentration of 2000 µg/mL. The aliquots were stored at -80°C.

Vemurafenib/PLX 4032 (Selleck, prod.no. s1267) was dissolved in DMSO to a stock concentration of 20 mM and aliquots were stored at -20°C.

2.3 2D-experiments

2.3.1 Monocultures

Melmet cells were diluted in RPMI+ and seeded out in 96-well plates (Nunclon Delta Surface, Thermo Scientific). Initially, varying cell numbers were added to each well to determine the optimal cell density for the assay. For both cell lines, 7000 cells per well were considered to be the optimal cell number.

2.3.2 Co-cultures

In this experiment we wanted to determine if lung fibroblasts affect the therapy response of vemurafenib and APG350 in melanoma cells.

The GFP-luc tagged Melmet cell lines (described in 2.1.1) were co-cultured with WI-38 fibroblast in EMEM medium, using 4000 cells of each cell type per well. Melmet cells cultured as mono-cultures in EMEM were used as control cells. The cells were seeded out on white, clear-bottomed 96-well plates (Corning® Flat clear bottom white microplate) and cultured in standard culturing conditions.

2.3.3 Treatment of 2D-cultures

The cells were treated with different concentrations of vemurafenib and/or APG350 depending on the analysis to follow. See table 2.3 for an overview of the drug concentrations used for the different experiments. Each drug concentration was performed in 3-8 parallels and the 96-well plates were incubated under normal culturing conditions for 72 hours before analysis. All drug dilutions were made in the medium optimized for the cell types used (table 2.2).

Table 2.3: Drug concentrations used in 2D-experiments.

2D-experiments	Concentration APG350 [µg/mL]	Concentration vemurafenib [µM]
Mono-therapy, dose response:	0,005 – 0,01 – 0,05 – 0,1 – 0,5 – 1 – 5 – 10 – 20 – 100	0,033 – 0,66 – 3,3 – 6,6 – 33 – 66 – 333 – 660
Combination therapy:	0,01 – 0,1 – 1	0,033 – 0,066 – 0,33 – 3,3
Conditioned medium:	0,1	0,33 – 3,3 – 6,6
Co-cultures:	0,1	0,33 – 3,3 – 6,6

2.3.3.1 Mono-therapy and combination therapy with vemurafenib and APG350

Mono-therapy of the cells was done to evaluate the effect of APG350 and vemurafenib alone. The results were acquired to evaluate dose response and to select the drug concentrations to be used for combination therapy. Twenty four hours after seeding the cells, the medium was removed and 100 μ l of fresh medium containing either of the drugs or both in combination was added. Since vemurafenib is diluted in DMSO, a control consisting of RPMI+ with DMSO was set up alongside the combination therapy wells. The amount of DMSO utilized was equivalent to the amount of vemurafenib used for each concentration. For an example of a setup used for combination therapy of monocultures see figure 2.2.

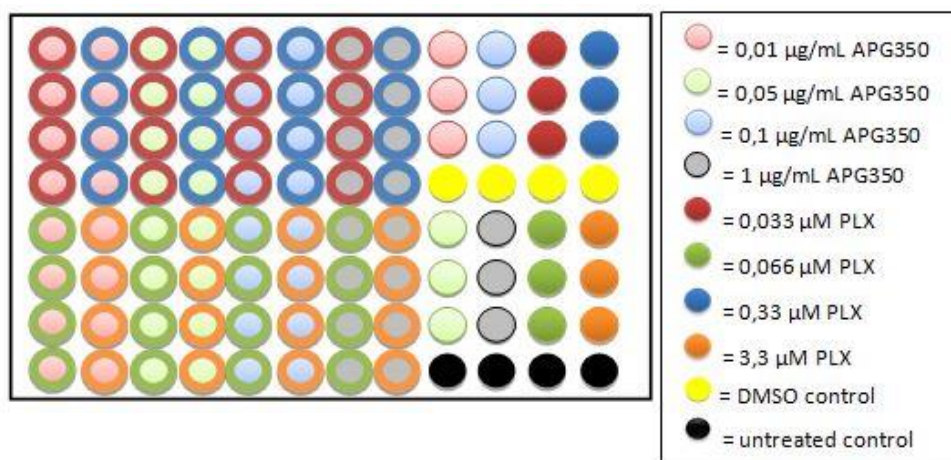


Figure 2.2: Example of a typical setup used for combination therapy of monocultures. The figure models a 96-well plate with combinations of APG350 and vemurafenib (PLX) in the first 8 columns and mono-therapy in the last 4 columns.

2.3.3.2 Conditioned medium infused with vemurafenib and APG350

To evaluate if normal fibroblasts secrete factors that affect the therapy response of melanoma cancer cells, an experiment was set up where Melmet cells were treated with vemurafenib and/or APG350 infused in fibroblast-conditioned medium. The cells were seeded out and cultured as described in chapter 2.3.1 and treated with drugs as described in the previous chapter. The drug dilutions were made in EMEM-medium (table 2.2), but the medium was conditioned before use. Cells treated with normal, non-conditioned medium were used as control cells.

Conditioned medium was prepared by culturing 500 000 WI-38 fibroblasts in EMEM medium for 72 hours under normal culturing conditions. The conditioned medium was filtered through a 0,45 μ m syringe filter to remove dead cells and debris. The medium was used directly after the filtration.

2.3.4 CalcuSyn analysis

The combined results of four 2D-combination therapy experiments were evaluated for possible synergy using the CalcuSyn data program (BioSoft, Feruson, MO, USA). Additionally, two 3D-experiment parallels were evaluated (chapter 2.4). The program uses the Chou and Talalay combination index (CI) to determine the interaction of two drugs (see appendix II for detailed info). The inputs were the doses and responses of mono-therapy and combination therapy at different ratios. Response-rates were given as dead cells relative to untreated control cells. All negative values, indicating increased cell survival, were excluded since the program only accepts positive values. Non-exclusive CI-values were used. Non-exclusive treatments are defined as treatments affecting different targets or different sites of the same target.

2.4 3D-experiments

Cells cultured as spheroids give a more realistic model of the cell-cell interactions seen *in vivo* compared to 2D-cell cultures³⁴. In this project, 3D-cultures in the format described by Vinci et al³³ were utilized. The results were used to evaluate and support the results from 2D-cultures.

2.4.1 Seeding of spheroids

To stimulate the formation of spheroids, Melmet 1 and Melmet 5 cells were suspended in RPMI+ and 200 μ L were seeded out in low attachment 96-well plates (Corning® 96 Well Clear Round Bottom Ultra Low Attachment Microplate). 3000 cells per well were used based on experiments previously performed by Solveig Pettersen. Melmet 1 cells do not form spheroids spontaneously and were therefore cultured in RPMI+ mixed with 2 % Matrigel. The spheroids were grown under normal culturing conditions for 72 hours before treatment with vemurafenib and/or APG350.

2.4.2 Treatment of spheroids

To determine the optimal drug concentrations to be used in therapy, spheroids were treated in mono-therapy with broad ranging concentrations of APG350 and vemurafenib and cultured for 14 days. Based on these results concentrations for combination therapy were chosen and set up in 6 parallels per drug dose. It was assessed that the spheroids were to be cultured in drug infused medium for 5 days. Table 2.4 shows the drug concentrations used in this experiment.

Table 2.4: *Drug concentrations used in 3D-experiments.*

3D-experiments	Concentration APG350 [μ g/mL]	Concentration vemurafenib [μ M]
Melmet 1:	0,5 – 5	0,33 – 3,3
Melmet 5:	0,5 – 5	0,066 – 0,33

2.4.3 Phase contrast imaging and measurement of spheroid radius

The spheroids were photographed and measured every day, five days a week. Pictures were taken with an Olympus IX81 microscope and the spheroids were measured using the Cell[^]P computer program. The mean cell radius was used to calculate the volume of each spheroid. The volume in mm³ was calculated for all spheroid parallels and the average spheroid volume for each therapy dose was calculated for each measurement day. These calculations were used to create growth curves depicting the spheroids growth from day to day. See appendix III for a calculation example of spheroid volume.

On the 5th day after treatment the spheroids were analyzed with the CellTiter-Glo[®] Luminescent Cell Viability-assay as described in chapter 2.5.2. Before the Glo-reagent was added the spheroids were transferred to black, flat-bottomed 96-well plates (Corning[®] 96 well Black Plate, Clear Bottom with lid) along with 50 μ L medium. Using opaque-welled plates is important to prevent the luminescent signals of each well to leak through to other wells. The medium and spheroids of each well was gently pipetted up and down to stimulate spheroid disintegration.

2.5 Cell Viability

2.5.1 CellTiter 96[®] AQueous One Solution Cell Proliferation Assay (MTS-assay)

The MTS-assay is a colorimetric assay for measuring the number of metabolically active cells in proliferation. MTS, or 3-(4,5-dimethylthiazol-2-yl)-5-(3-carboxymethoxyphenyl)-2-(4-sulfophenyl)-2H-tetrazolium, is a compound that (together with the electron coupling reagent phenazine ethosulfate (PES)) is reduced by dehydrogenase enzymes found in metabolically active cells to form a formazan product which is soluble in tissue culture medium. The formazan product gives a copper-brown solution and can be quantified by measuring the absorbance at 490 nm. The amount of formazan is directly proportional to the number of living cells in culture⁵⁸.

All monocultured cells used in 2D-experiments were analyzed with the MTS-assay, except conditioned medium treated cells. 20 μ L of MTS reagent was added to each well, including a column of wells containing only cell medium (no cells) used to read background absorbance. The plate was incubated under normal culturing conditions for 1 hour. The absorbance at 490 nm was measured with a micro plate reader (Wallac Victor²), and the relative viability in % was calculated setting the absorbance of untreated control cells as 100 %.

2.5.2 CellTiter-Glo[®] Luminescent Cell Viability-assay

The Cell-Titer-Glo[®] Luminescent assay, hereby called the Glo-assay, is a method used to determine the number of viable cells in culture based on quantification of ATP, an indicator of metabolically

active cells. The amount of ATP present in the cell culture is directly proportional to the number of cells present in culture⁵⁹. The Glo-assay relies on the generation of a stable luminescent signal catalyzed by a thermo-stable luciferase. In the presence of Mg^{2+} , ATP and molecular oxygen, the substance beetle luciferin is oxidized to oxyluciferin which gives a stable luminescent signal⁶⁰. The reaction is shown in figure 2.3.

The Glo-assay was performed on all 3D-cultures as well as the experiments where conditioned medium was utilized. The 96-well plates were temperate to room temperature for 30 minutes before 50 μ L medium was removed from each well and 50 μ L of CellTiter-Glo®-reagent was added (1:1). The plates were mixed for approximately 2 minutes on a plate shaker and left for 10-15 minutes in room temperature before reading luminescence (1s/well) on the Wallac Victor²-plate reader.

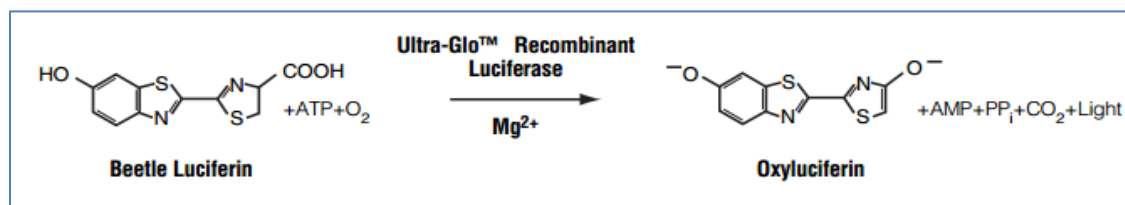


Figure 2.3: The figure illustrates the oxidation of beetle luciferin to oxyluciferin in the presence of a thermo-stable luciferase, Mg^{2+} , ATP and O_2 . Emission of light can be measured as luminescence and is proportional to the amount of ATP present. The figure is adapted from the Promega CellTiter-Glo Luminescent Cell Viability Assay protocol⁶⁰.

2.5.3 Luciferase-assay

By adding D-luciferin to cells expressing luciferase, you get the substance oxyluciferin and light in an energy demanding reaction (figure 2.3). Only living cells will express luciferase, therefore the amount of light produced is proportional to living cells in culture.

The luciferase-assay was used on the co-culture experiments. 1 μ L of luciferin-solution was mixed with 199 μ L RPMI and added to each well. The wells were previously emptied of the drug infused medium. The plate was left for 10 minutes in room temperature before reading luminescence (1s/well) on the Wallac Victor²-plate reader. Refer to appendix IV for the protocol on how to make luciferin-solution.

2.6 Western Immunoblotting

The Western blot is a method used to detect specific proteins in a sample. Gel-electrophoresis separates proteins according to mass and charge, and the proteins are blotted from the gel to a membrane using an electrical gradient. Proteins on the membrane can be detected by e.g. antibodies,

as is usual in Western immunoblotting. The primary antibody can either be directly conjugated to an enzyme, for instance horse radish peroxidase (HRP), or to a secondary antibody conjugated to HRP (figure 2.4). Antibody-antigen interactions are specific and therefore allow target proteins to be detected in complex protein mixtures.

In this project, membranes were set up with cell lysates from three different biological experiments.

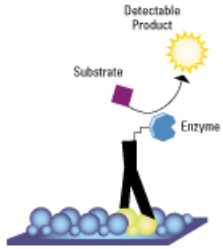
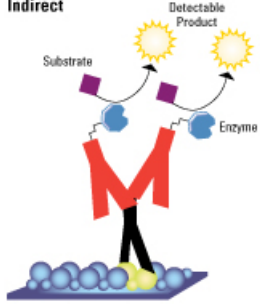
<p>Direct</p> 	<p>Advantages</p> <ul style="list-style-type: none"> • Quicker since only one antibody is used • No concern for cross-reactivity of a secondary antibody • Double possible with different labels on primary antibodies <p>Disadvantages</p> <ul style="list-style-type: none"> • Labeling may reduce immunoreactivity of primary antibody • Labeled primary antibodies are expensive • Low flexibility in choice of primary antibody label • Little signal amplification
<p>Indirect</p> 	<p>Advantages</p> <ul style="list-style-type: none"> • Secondary antibody can amplify signal • A variety of labeled secondary antibodies are available • One secondary may be used with many primary antibodies • Labeling does not affect primary antibody immunoreactivity • Changing secondary allows change of detection method <p>Disadvantages</p> <ul style="list-style-type: none"> • Secondary antibodies may produce nonspecific staining • Additional steps required compared to the direct method

Figure 2.4: Advantages and disadvantages of direct vs. indirect detection methods used in Western blotting. The figure is adapted from Thermo Scientific⁶¹.

2.6.1 Culturing, treatment and harvesting of cells for Western Immunoblotting

Protein lysates were prepared from both Melmet cell lines. Twenty four hours after seeding $4,0 \cdot 10^5$ Melmet 1 or Melmet 5 cells in T25 flasks, the cells were treated with APG350 and/or vemurafenib, concentrations are presented in table 2.5. The cells were treated for 24 hours before harvesting.

The cells were harvested using a cell scraper, and the cells and the medium were transferred to 15 mL tubes, centrifuged at 1000 rpm for 5 minutes and the cell pellets re-suspended in ice cold PBS. The cells were transferred to eppendorf tubes, centrifuged at 2000 rpm for 4 min. and the PBS removed. The cells were kept on ice during the procedures to stop signaling pathways and inhibit protein degradation. The cell pellets were frozen at -80°C .

Table 2.5: Drug concentrations used to treat cells for Western Immunoblotting.

Western Immunoblot	Concentration APG350 [$\mu\text{g/mL}$]	Concentration Vemurafenib [μM]
Melmet 1	0,1	0,33 – 0,66 – 3,3
Melmet 5	0,1	0,33 – 0,66 – 3,3

2.6.2 Protein lysates

The cells were lysed by adding lysis buffer (appendix V) containing protease and phosphatase inhibitors following incubation on ice for 1 hour with vortexing every 15 minutes. The samples were sonicated for 5 seconds and centrifuged at 13000 rpm for 10 minutes at 4°C to separate cell membrane components from the proteins. The supernatant consisting of the protein lysate was transferred to eppendorf tubes and frozen at -80°C.

2.6.3 Measurement of protein concentration

To load an equal amount of protein in each well of the gel, the protein concentration of each sample was decided. The protein concentration was measured using the Pierce BCA Protein Assay Kit (Thermo Scientific), a colorimetric assay based on the biuret reaction (reducing Cu^{2+} to Cu^{1+} in an alkaline medium) where Cu^{1+} is detected using a reagent containing bicinchoninic acid (BCA). The reaction product is purple-colored and water soluble and exhibits a strong absorbance at 562 nm. According to the producer the absorbance is nearly linear with increasing protein concentrations from 20 – 2000 $\mu\text{g/mL}$ ⁶².

Standards with concentration from 0 – 2000 $\mu\text{g/mL}$ were prepared according to the producers' protocol, and the samples were diluted in lysis buffer (5 μL sample + 55 μL lysisbuffer). The samples and standards were set up in duplicates. The BCA working reagent was prepared by mixing 50 parts of BCA Reagent A with 1 part of BCA Reagent B and 200 μL was added to the samples and standards. The samples and standards were incubated at 37°C for 30 minutes and the absorbance was measured at 540 nm, 1s/well, on the Wallac Victor² plate reader. The protein concentration was calculated from a standard curve based on the absorbance of the standards (0-2000 $\mu\text{g/mL}$). Refer to appendix VI for an example of a standard curve with calculations of protein concentration and volume to be applied on gels.

2.6.4 NuPAGE® Bis-Tris Electrophoresis System

The NuPAGE® Bis-Tris Electrophoresis System is an improved version of the well-known SDS-PAGE system, short for Sodium Dodecyl Sulfate PolyAcrylamide Gel Electrophoresis. SDS is an

anionic detergent used to denature proteins and to impart a negative charge to the proteins. This is important so that proteins of the same mass move at the same speed through the gel matrix toward the anode independent of their former secondary, tertiary and quaternary structure. The polyacrylamide gels are made up of a meshwork of fibers forming pores, and the density of the gel will determine the proteins speed when wandering through the gel.

In this project we used Life Technologies Novex® NuPAGE® SDS-PAGE gel system. The commercial gels are made with Bis-Tris/HCl buffer and SDS is added in the Running Buffer. To denature and reduce protein disulphide bonds a loading buffer containing LDS (Lithium Dodecyl Sulphate), equivalent to SDS, is added and heated to 70°C. The system provides a neutral pH environment during electrophoresis which according to the producer gives a better resolution and stability than older systems.

Commercial gels with increasing density of polyacrylamide (4-12 %) were used (Invitrogen). The gels were loaded with 10 µg sample; the volume of each sample was calculated from the sample concentration and diluted with lysis buffer to a total of 10µL (Appendix VI). Loading buffer was made by mixing 2,5 µL LDS Sample Buffer (4x) with 1 µL Sample Reducing Agent (10x), and this was added to the samples. The samples were denatured at 75°C for 10 minutes before application on the gel. 2,5 µL SeeBlue standard, a molecular weight marker, was added to the first and last well of the gel. The electrophoresis was run in 1x MES for 60 minutes at 150 V on an invitrogen PowerEase™500 electrophoresis machine.

2.6.5 Blotting

All Western blot experiments performed in this project was executed using the dry-blotting system⁶³. The transfer of proteins from a gel to a membrane is executed by placing a top and bottom blotting stack above and under the gel as shown in figure 2.5. The dry-blotting system differs from the traditional wet-blotting by being a more efficient, plug-and-play system with no need for additional buffers.

The gels were blotted onto 0,2 µm nitrocellulose membranes using the iBlot™ blotting machine. The blot was executed for 8 minutes using a voltage of 23 V.

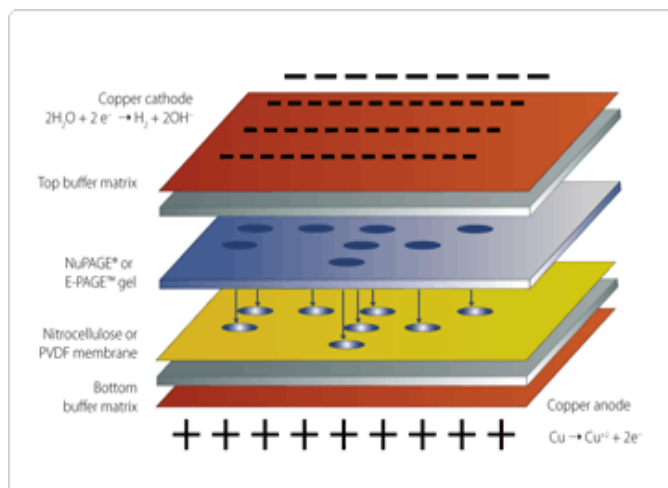


Figure 2.5: Blotting stack. The top stack includes a copper cathode and a buffer matrix containing the necessary ions to create an electrical current. The bottom stack contains a copper anode, a buffer matrix and a nitrocellulose membrane to which the proteins are transferred. The NuPAGE gel is situated in the middle. The figure is acquired from Life Technologies web page⁶⁴.

2.6.6 Immunodetection

The membranes were incubated with selected primary antibodies to detect the protein of interest, and these were visualized with secondary antibodies linked to HRP. HRP uses hydrogen peroxide as an oxidizing agent to oxidize its substrate. The substrate is found in the development solution SuperSignal® West Dura Extended Duration Substrate kit (Thermo Scientific) and chemoluminescence is produced by the reaction. Refer to table 2.6 and 2.7 for primary and secondary antibodies used in this experiment.

Before the membranes were incubated with a primary antibody they were blocked using a buffer consisting of 25mM Tris with pH 7,5 along with 0,15M NaCl and 0,1 % Tween (from here on called R&D-buffer, see Appendix VII) which was mixed with milk powder to a 5 % solution. The milk solution prevents unspecific binding of the primary antibody and thereby reduces background noise. The membranes were incubated in milk solution for 60 minutes and then treated with a primary antibody in a 2 % milk or BSA solution over night at 4°C.

The membranes were washed 3x10 minutes in R&D-buffer before they were incubated with secondary antibody in a 2 % milk solution for 60 minutes. The membranes were washed 3x10 minutes in R&D-buffer after the incubation. Washing and incubation was performed with continuous gentle agitation.

The proteins on the membranes were visualized by adding SuperSignal® Solution (Thermo Scientific) and quantified using the G_Box (Syngene, England) and the software GeneSnap version 7.12 (Syngene, England).

Some membranes were stripped of antibodies and re-incubated with a different antibody. The membranes were incubated in a stripping solution for 10 minutes with gentle agitation. The stripping solution was removed and the membrane rinsed in R&D-buffer before the procedure of blocking and incubation with new primary and secondary antibody was repeated. Refer to appendix VIII for details about the stripping solution.

Table 2.6: Primary antibodies used for immunodetection on Western blots.

Primary antibody	Dilution	Company, cat. #
Alpha-tubulin (mouse)	1:1000	Sigma, #T9026
Bad (rabbit)	1:500	Cell Signaling, #9292
Bid (rabbit)	1:1000	Cell Signaling, #2002S
Bim (rabbit)	1:1000	Cell Signaling, #2933S
Casp-3(rabbit) pro-casp. + cleaved casp.	1:1000	Cell Signaling, #9664S, #9662S
Casp-8 (mouse)	1:500	Alexis, ALX-804-242
Casp-9 (rabbit)	1:500	Cell Signaling, #9502
Mcl-1 (rabbit)	1:500	Cell Signaling, #4572S
PARP (rabbit)	1:500	Cell Signaling, #9542
pERK 1/2 (rabbit)	1:1000	Cell Signaling, #9102
pBad Ser112 (rabbit)	1:500	Cell Signaling, #5284S
pBad Ser136 (rabbit)	1:1000	Cell Signaling, #4366S
Smac/DIABLO (mouse)	1:1000	Cell Signaling, #2954S

Table 2.7: Secondary antibodies used for immunodetection on Western blots.

Secondary antibody	Dilution	Company, cat. #
Rabbit anti-mouse	1:3000	Dako, P0260
Goat anti-rabbit	1:3000	Dako, P0448

2.7 PuMA-assay

PuMA, short for pulmonary metastasis assay, is an *ex vivo* assay developed to show the metastatic progression of GFP-expressing cancer cells in the mouse lung environment in real-time⁶⁵. There has been a need for an assay that depicts how metastatic progressions from single cells to metastatic lesions at secondary sites occur. Simple *in vitro* assays do not provide a sufficient model of the complex interactions taking place between cancer cells and the tumor microenvironment in regards to metastasis. Also, *in vivo* models for the most part provide end point outcomes of metastasis. The

PuMA-assay is a simple assay that allows one to follow the process of metastatic progression at a secondary site over time. Lung tissue provides a 3D collagen network with associated lung epithelial cells, inflammatory cells and other stromal elements in which GFP-expressing cancer cells interact⁶⁵. Images can be acquired from day to day and the GFP-expressing cells quantified.

In this study the PuMA-assay was used in the evaluation of therapeutic response at different time points after metastatic progression and in an environment with different cells surrounding the cancer cells; the tumor microenvironment. Lung tissue from an “athymic nude foxn1 nu” mouse infused with Melmet 5 GFP-tagged cells was provided and prepared by Karianne Fleten at the Department of Tumor Biology. The Melmet 5 GFP-tagged cells were injected intravenously into the mouse through the tail (figure 2.6). The mouse was humanely euthanized with an overdose of Pentobarbital 15 minutes after cell infusion, and the lung was injected with 1,2 % low melting agarose mixed 1:1 with PuMA 2x medium (appendix IX). The lungs were removed from the mouse, cooled in PBS supplemented with Penicillin/Streptomycin to a concentration of 100 U/mL and cut by hand into tissue section with approximately the same thickness.

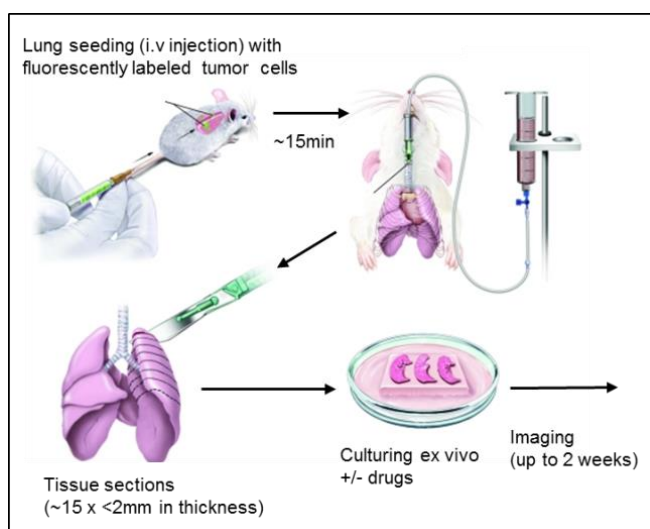


Figure 2.6: Illustration of PuMA assay preparations. Melmet 5 GFP-tagged cells are injected intravenously through the mouse tail. The lung was injected with an agarose/PuMA-medium mix, removed from the mouse and tissue sections cut and cultured ex vivo. Image adapted from Mendoza et.al.⁶⁵.

The tissue sections were placed individually onto small squares of Gelfoam® situated in wells of a 24-well plate. A volume of 300 μ L PuMA 1x medium (appendix IX) infused with different doses of vemurafenib and/or APG350 was added to the wells (table 2.8). The concentrations of vemurafenib were chosen based on the results from 2D- and 3D-experiments as well as previous PuMA-results from other members of the group. Untreated control tissue and DMSO treated tissue was included as controls. All treatments were set up in two parallels (two tissue sections) and were incubated in standard culturing conditions. The medium was changed every Monday, Wednesday and Friday and the tissue sections turned on the same days. The lung tissue was cultured for a total of 13 days.

Table 2.8: Drug concentrations used in treatment of mouse lung tissue for the PuMA-assay.

PuMA-assay	Concentration APG350 [$\mu\text{g/mL}$]	Concentration Vemurafenib [μM]
Mouse lung tissue infused with Melmet 5-GFP cells	1 – 5	0,066

2.7.1 Phase contrast and fluorescent imaging, quantification of fluorescence intensity and immunohistochemistry staining

Phase contrast and fluorescent images were taken from two different areas of each lung tissue section three times a week, resulting in 2 parallel sections x 2 areas of each section = 4 photographs of each given treatment.

Quantification of fluorescence intensity was performed using the Java based image processing program ImageJ, version 1.43m, developed by Wayne Rasband at the National Institutes of Health, USA. The color photographs were transformed to 8-bit grey scale pictures and the threshold was adjusted for each picture so that background fluorescence was not included in the calculations. A defined area (ROI) was set and quantification limited to this area on all tissue pieces. It was endeavored to localize the same area for quantification for every tissue piece from day to day. Particles in the ROI were analyzed for the fluorescence intensity, but particles smaller than 50 pixels were excluded from the calculations.

Fluorescence intensity was measured as integrated density, a parameter representing colony area multiplied with mean pixel intensity. By summing together the integrated density of each colony we got a number representing the fluorescence intensity in the given ROI. The average intensity of all four photographs of a given treatment was calculated and the results were set relative to the control tissue, making the numbers comparable in the graphs. The results give an indication of colony growth from day to day.

The tissue sections were fixated in 4 % formalin after 13 days of culturing and sent to immunohistochemistry staining at The Norwegian Radium Hospital, Department of Pathology. The stained sections were visually inspected and photographed using the Olympus BX51 system microscope and Cell[^]P computer program.

3. Results

3.1 The sensitivity of Melmet cells to vemurafenib and APG350

3.1.1 Mono-therapy in 2D-cultures

The dose response of the mutated BRAF inhibitor vemurafenib and TRAIL receptor agonist APG350 was evaluated in Melmet 1 and Melmet 5 (Figure 3.1).

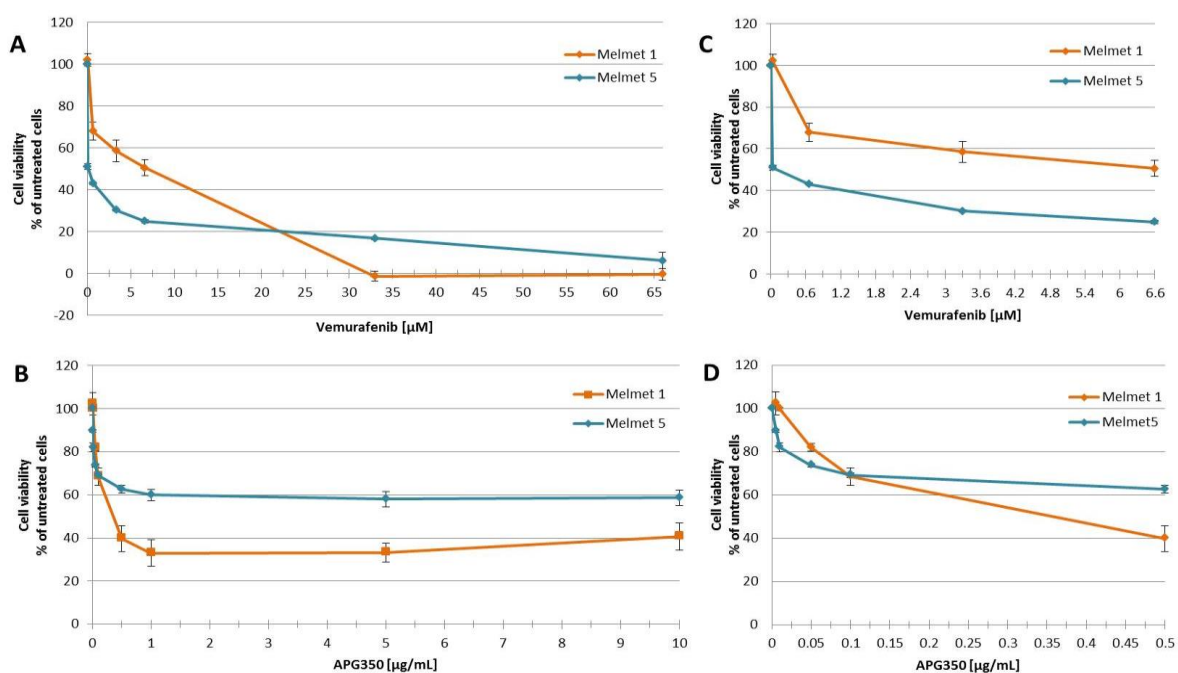


Figure 3.1: The sensitivity of Melmet 1 and Melmet 5 to vemurafenib (A) and APG350 (B). Graph C and D are enlargements of the lowest data points in graph A and B respectively. All graphs show viable Melmet cells in % of untreated cells. The data points are an average of two and three independent biological experiments and standard error of the mean (SEM) is shown.

Both cell lines show decreased cell viability with increasing concentrations of vemurafenib, indicating that both cell lines are sensitive to the drug (Figure 3.1 A). The graphs show differences in dose response; at low concentrations Melmet 1 is less sensitive to the drug than Melmet 5, with a median lethal dose (LD_{50}) at approximately 6,6 μM vs. approximately 0,03 μM for Melmet 5 (figure 3.1 C). With vemurafenib doses higher than approximately 22 μM the situation is turned and the drug kills more Melmet 1 cells than Melmet 5 cells. All Melmet 5 cells were treated with vemurafenib concentrations up to 660 μM , but there was no additional effect above 66 μM .

APG350 induces a dose dependent cell killing in both cell lines indicating that they both are sensitive to the agent. Melmet 1 has a better response than Melmet 5; a dose of 1 $\mu\text{g}/\text{mL}$ killing approximately

65 % of the Melmet 1 cells vs. 40 % of the Melmet 5 cells (figure 3.1 B). Increasing the dose further does not seem to give any additional effect. Rather, it seems that APG350 concentrations above 5 $\mu\text{g}/\text{mL}$ may increase cell survival in the Melmet 1 cell line, as is indicated in the increase of the curve in figure 3.1 B. All Melmet 5 cells were treated with APG350 doses up to 100 $\mu\text{g}/\text{mL}$ but there was no additional effect above 5 μM . Figure 3.1 D shows the lowest data points from figure 3.1 B enlarged.

Vemurafenib is dissolved in DMSO, and the effect of DMSO on cell survival is presented in figure 3.2. DMSO increases cell survival in both cell lines.

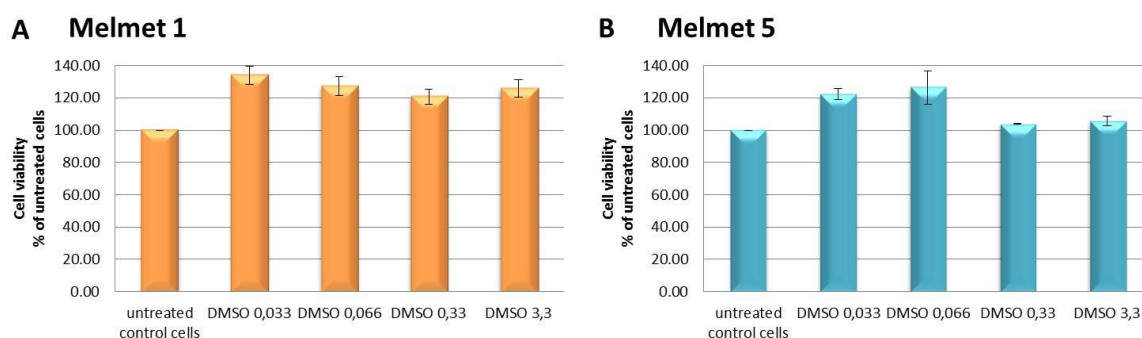


Figure 3.2: DMSO controls of Melmet 1 (A) and Melmet 5 (B) shown as viable cells in % of untreated cells. Four different DMSO-concentrations were analyzed, where the amount of DMSO utilized was equivalent to the vemurafenib volume used for each given concentration in the combination therapy experiments. The data points are an average of three individual biological experiments and SEM is shown.

3.1.2 Combination therapy in 2D-cultures

Based on the dose response results, concentrations of each drug were chosen for combination therapy (Table 2.3 in chapter 2.3.3). The results of the combination therapy with vemurafenib and APG350 are shown in figure 3.3.

The Melmet 1 cells response to combination therapy varies depending on the concentration of APG350 and vemurafenib utilized (figure 3.3 A). All the tested doses of APG350 combined with low vemurafenib doses interestingly give an increase in cell survival compared to APG350 mono-therapy (presented as data points $x = 0$). When increasing the vemurafenib doses to 0,33 μM and higher, APG350 0,1 $\mu\text{g}/\text{mL}$ (purple graph) reduces cell viability relative to mono-therapy, but all other combinations do not induce any additional effect. The results imply that combination therapy on Melmet 1 is not effective at most concentrations tested in this study.

Melmet 5 cells respond to combination therapy with increased cell death compared to mono-therapy in most of the tested concentrations (figure 3.3 B). All doses of vemurafenib combined with APG350 0,1

$\mu\text{g/mL}$ and $1 \mu\text{g/mL}$ induces prominent additional effects of combination therapy. APG350 $0,01 \mu\text{g/mL}$ (red graph) is the only tested dose that causes cell survival in combination with all the tested vemurafenib doses when comparing to vemurafenib mono-therapy. This dose also causes cell survival compared to APG350 mono-therapy when combined with the lowest vemurafenib concentration. All other combinations give a markedly better effect than mono-therapy.

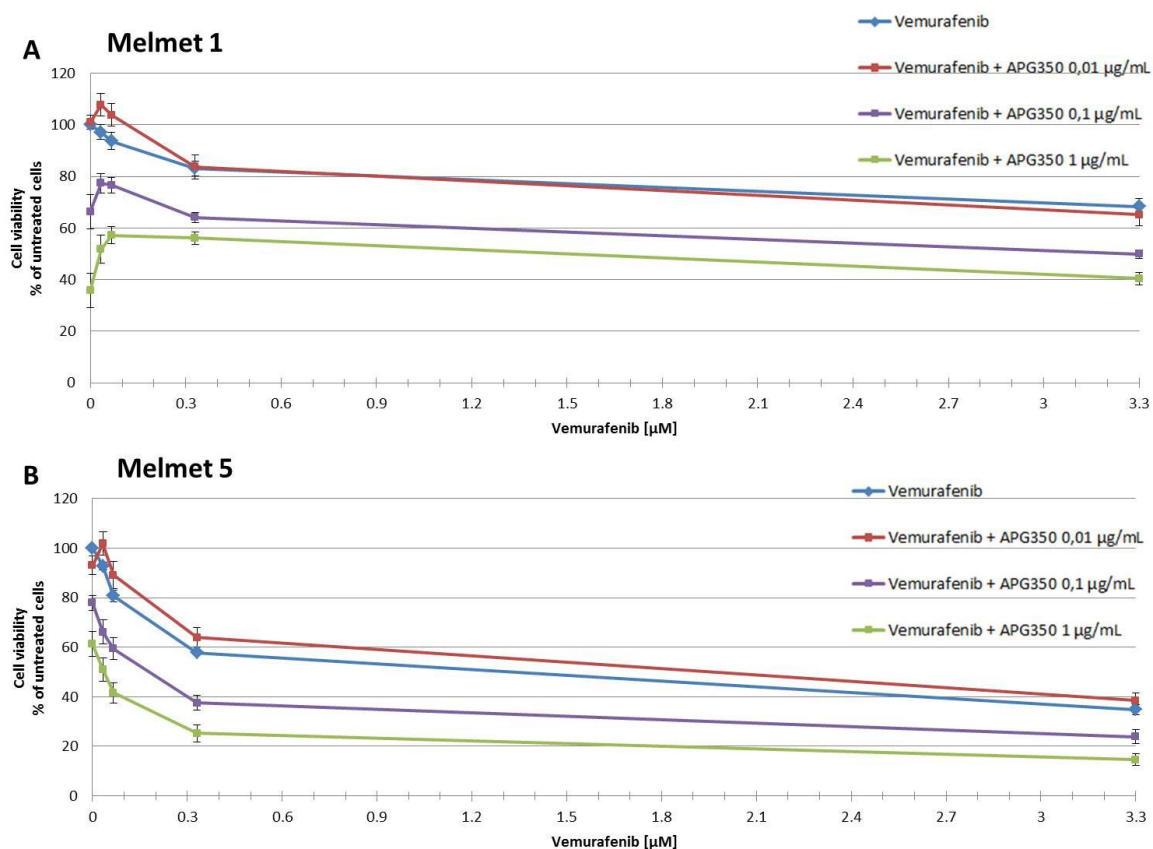


Figure 3.3: Melmet 1 (A) and Melmet 5 (B) treated with combinations of vemurafenib and APG350. The graphs show viable Melmet cells in % of untreated cells. Vemurafenib is shown on the x-axis and the different colored curves each represent a concentration of APG350. The blue graphs show cells treated with vemurafenib as mono-therapy. The red graphs show cells treated with vemurafenib combined with APG350 $0,01 \mu\text{g/mL}$. The purple graphs show vemurafenib combined with $0,1 \mu\text{g/mL}$ APG350 and the green graphs show vemurafenib combined with $1 \mu\text{g/mL}$ APG350. The data points at $x = 0$ show APG350 in mono-therapy. The data points are an average of four independent biological experiments and standard error of the mean (SEM) is indicated. Refer to Appendix Xa for combination therapy graphs presented as column charts.

CI-values were calculated to evaluate if the different combinations of drugs give a synergistic, additive or antagonistic effect (table 3.1). The CI-values for Melmet 1 show that only one combination of APG350 with vemurafenib, $0,1 \mu\text{g/mL} + 3,3 \mu\text{M}$, induces synergy, while the rest give antagonistic or additive effects. These results are consistent with the combination therapy graphs in figure 3.3 A which indicate that combining the two drugs in most cases will not give any additional effect compared to mono-therapy.

For Melmet 5, CI-values for the lowest APG350 concentration (0,01 µg/mL) combined with all calculated vemurafenib concentrations give antagonistic or additive results, with CI-values of near 1 and higher. All the other drug combinations give synergistic effects. The combination giving the best combined effect seem to be vemurafenib 0,33 combined with APG350 1 µg/mL. The results of these calculations are consistent with what was seen in figure 3.3 B.

Table 3.1: CI-values calculated for Melmet 1 and Melmet 5 based on the 2D-combination therapy results. Values <1 indicate synergism, values = 1 imply additive effects and values >1 indicate antagonism. Calculations of CI-values were excluded in the cases where combination therapy gave increased survival relative to untreated cells, as described in Materials and methods chapter 2.3.4.

Melmet 1

APG350 [µg/mL]	Vemurafenib [µM]	CI-values
0,01	0,033	excluded
0,01	0,066	excluded
0,01	0,33	1,4
0,01	3,3	1,3
0,1	0,033	2,6
0,1	0,066	2,5
0,1	0,33	1,0
0,1	3,3	0,7
1	0,033	3,2
1	0,066	4,8
1	0,33	4,7
1	3,3	1,9

Melmet 5

APG350 [µg/mL]	Vemurafenib [µM]	CI-values
0,01	0,033	excluded
0,01	0,066	3,2
0,01	0,33	0,9
0,01	3,3	1,8
0,1	0,033	0,3
0,1	0,066	0,3
0,1	0,33	0,2
0,1	3,3	0,6
1	0,033	0,6
1	0,066	0,3
1	0,33	0,1
1	3,3	0,3

3.1.3 Mono-therapy and combination therapy in 3D-cultures

Melmet cells cultured as spheroids were treated with vemurafenib, APG350 or a combination of these for 96 hours. Spheroid growth, measured as cell volume in mm³ from day to day, is depicted as growth curves and microscope pictures in figure 3.4.

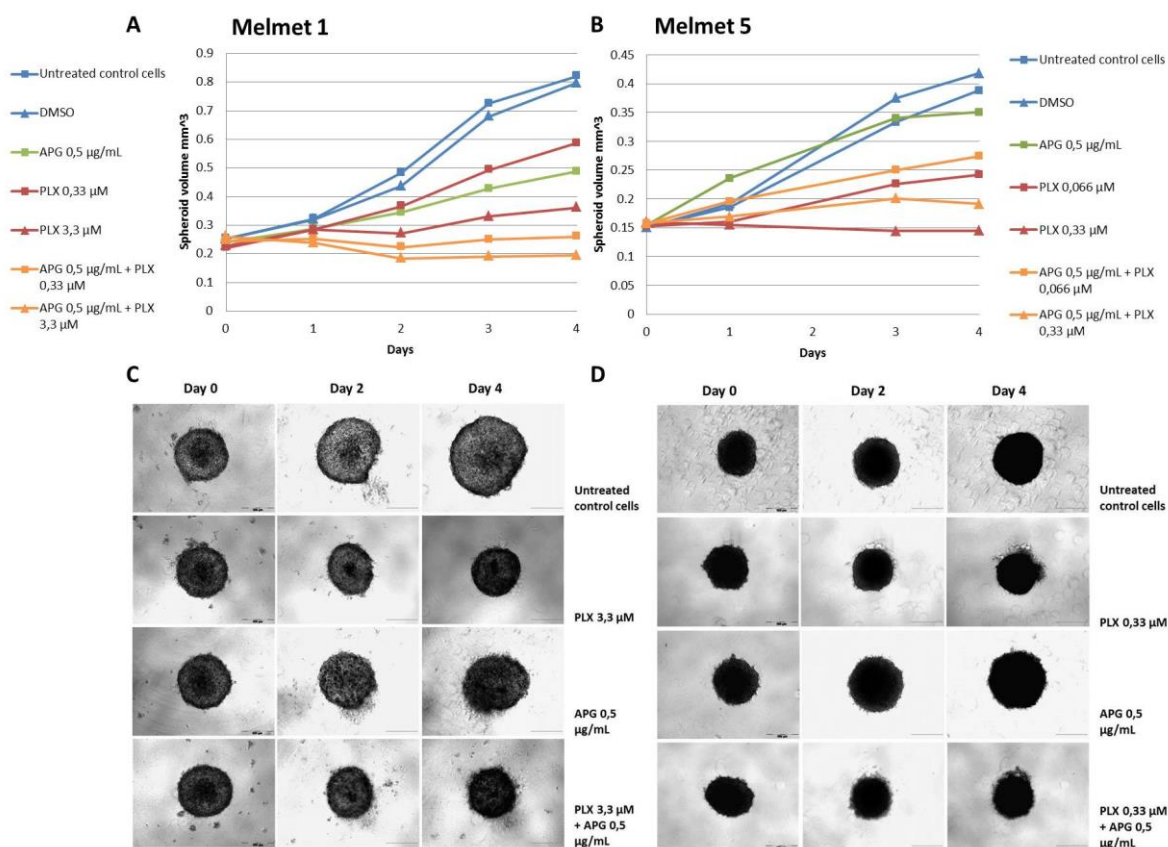


Figure 3.4: Growth of Melmet 1 (A&C) and Melmet 5 (B&D) spheroids cultured over 96 hours with different concentrations of vemurafenib (PLX) and APG350 (APG). The curves (A&B) show spheroid growth on each day as spheroid volume in mm^3 . The data points are an average of two independent biological experiments, where each drug concentration/control was set up with 6 parallels. Blue curves indicate control cells, red curves indicate vemurafenib treatment, green indicate APG350 treatment and orange indicate combination treatments. Note that Melmet 1 and Melmet 5 spheroids are treated with different concentrations of vemurafenib. Photographs of Melmet 1 (C) and 5 (D) depict spheroid growth on selected days with selected treatment concentrations. See Appendix Xb for growth curves including all tested concentrations.

In Melmet 1 (figure 3.4 A), mono-therapy and combination therapy inhibits spheroid growth compared to untreated control spheroids, with combination therapy giving the most reduction in spheroid volume. The growth curves show that the untreated control spheroids and the DMSO control spheroids (blue lines) increase their volume at approximately the same rate. The mono-therapy APG350 treated spheroids (green line) increase their volume during the whole time period, but are significantly smaller than the control spheroids. The vemurafenib treated spheroids (red lines) show dose dependent growth, with the highest vemurafenib dose giving further reduced volume compared to the lowest vemurafenib dose. Combination therapy (orange lines) induces reduction in spheroid volume compared to the other therapies and control cells, and additionally inhibits growth to the extent that no gain in volume is seen during the period of the experiment. For the highest combination dose the spheroid volume is reduced from day 0 to day 4. The experiment included spheroids treated with an APG350 dose of 5 $\mu\text{g/mL}$

(curves not shown, see Appendix Xb), and this treatment did not give any difference in spheroid volume compared to APG350 0,5 µg/mL, neither in mono-therapy or in combination with vemurafenib.

The Melmet 5 growth curves (figure 3.4 B) show that combination therapy (orange lines) inhibits spheroid growth compared to control spheroids (blue lines), but that vemurafenib as mono-therapy (red lines) is more effective when comparing to similar doses of combination therapy. The highest concentration of vemurafenib mono-therapy is the most effective of the tested drugs and doses in regard to reducing spheroid volume. Untreated control spheroids and DMSO control spheroids increase their volume at approximately the same rate. Interestingly, spheroids treated with APG350 seem to grow better than the control spheroids for the first days, with no visible effect of the drug until day three and four. As for the Melmet 1 spheroids, the experiment included spheroids treated with 5 µg/mL of APG350; this treatment dose gave approximately similar spheroid volume as APG350 0,5 µg/mL, but differed in combination therapy (data not shown, see Appendix Xb).

Figures 3.4 C and D show selected microscope pictures of spheroids from day 0 to day 4. The Melmet 1 control spheroids increase their size more than Melmet 5 during the period of the experiment. Additionally, they are visually less dense and seem more “loose” than the Melmet 5 cells. Both cell lines show a reduction in volume compared to control spheroids when treated with drugs. The exception may be APG350 mono-therapy in Melmet 5, where a difference is hard to differentiate.

Cell viability of the spheroids on day 4 was evaluated using the Glo-assay (chapter 2.5.2). The results are presented in Figure 3.5. In both Melmet 1 and 5 the Glo-results indicate that combination therapy gives an additional effect compared to mono-therapy. For Melmet 1 this is consistent with what was seen in the growth curves (figure 3.4 A), but differ from the 2D-results (figure 3.3 A). For Melmet 5, the Glo-results differ from the growth curves (figure 3.4 B), but are consistent with the 2D-results (figure 3.3 B). CI-values calculated from the Glo-data confirm that all tested concentrations give synergistic effects (table 3.2).

Comparing figure 3.5 A and B in regard to dose response confirms the findings from 2D-cultures that Melmet 1 is more sensitive to APG350 than Melmet 5 is. Interestingly, the results also show that Melmet 1 is more sensitive to vemurafenib than Melmet 5, this being opposite of what was seen in the 2D-cultures. The Glo-results showed, like the growth curves, that a higher APG350 concentration (5 µg/mL, curves not shown) does not give any increased effect compared with 0,5 µg/mL of APG350 (Appendix Xc).

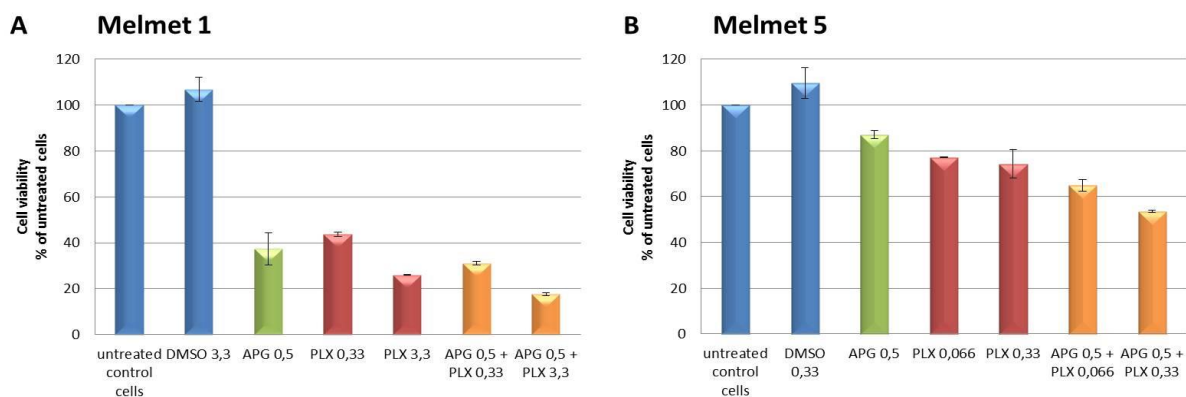


Figure 3.5: Melmet 1 spheroids (A) and Melmet 5 spheroids (B) analyzed with the Glo-assay after 96 hours of culturing in drug-infused medium. APG350 (APG) concentrations are given in $\mu\text{g/mL}$, vemurafenib (PLX) concentrations are given in μM . Note that Melmet 1 and Melmet 5 cells are treated with different vemurafenib concentrations. A DMSO control was included where the amount of DMSO utilized was equivalent to the vemurafenib volume used for the highest analyzed vemurafenib concentration. Each column represents the average of two individual biological experiments showing the cell viability in % of untreated cells. Standard error of the mean (SEM) is indicated. Selected treatment concentrations are shown; see Appendix Xc for all concentrations used in the experiment.

Table 3.2: CI-values calculated from the Glo-data of Melmet 1 and Melmet 5 spheroids. All values indicate synergism (< 1).

Melmet 1

APG350 [$\mu\text{g/mL}$]	Vemurafenib [μM]	CI-values
0,5	0,33	0,3
0,5	3,3	0,3

Melmet 5

APG350 [$\mu\text{g/mL}$]	Vemurafenib [μM]	CI-values
0,5	0,066	0,0
0,5	0,33	0,0

3.2 Protein expression in Melmet cells treated with vemurafenib and APG350

Western analysis was performed to evaluate the molecular response related to apoptosis in cells treated with combination therapy compared to cells treated with mono-therapy or cells without treatment. Proteins belonging to the extrinsic apoptotic pathway, activated by e.g. TRAIL-ligand binding, are presented in figure 3.6.

Procaspase-8 shows a higher degree of cleavage in combination therapy compared to mono-therapies and control samples in Melmet 1, while in Melmet 5 it seems that the protein is most cleaved in APG350 treated cells. The cleavage of procaspase-3 is in both cell lines most pronounced in cells exposed to combination therapy. Notably, the expression of the 12 kDa active caspase-3 band is stronger in both cell lines (figure 3.6 A and B). Also PARP, which is cleaved by caspase-3, has a higher degree of cleavage after the combination therapy.

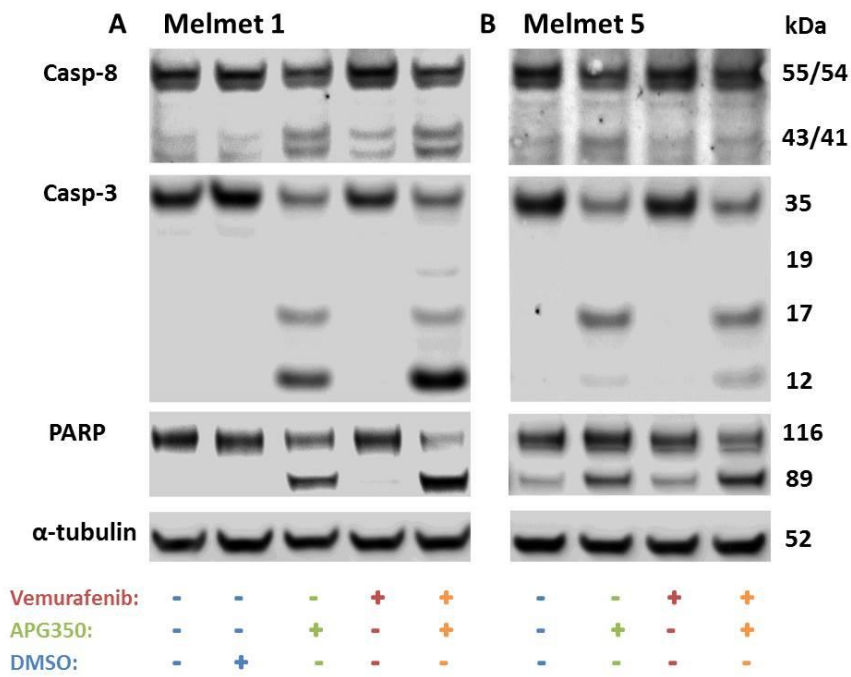


Figure 3.6: Western blots showing protein expression in Melmet 1 (A) and Melmet 5 (B). The blots presented are representative for three different biological experiments. DMSO controls were not included for the Melmet 5 cells in the shown parallel, but were included in the other parallels. The APG350 concentration = 0,1 μ g/mL. The vemurafenib concentration = 0,33 μ M.

Protein members of the intrinsic apoptotic pathway are shown in figure 3.7. Investigation of the expression of these proteins gives an indication of how the different drug treatments affect this pathway.

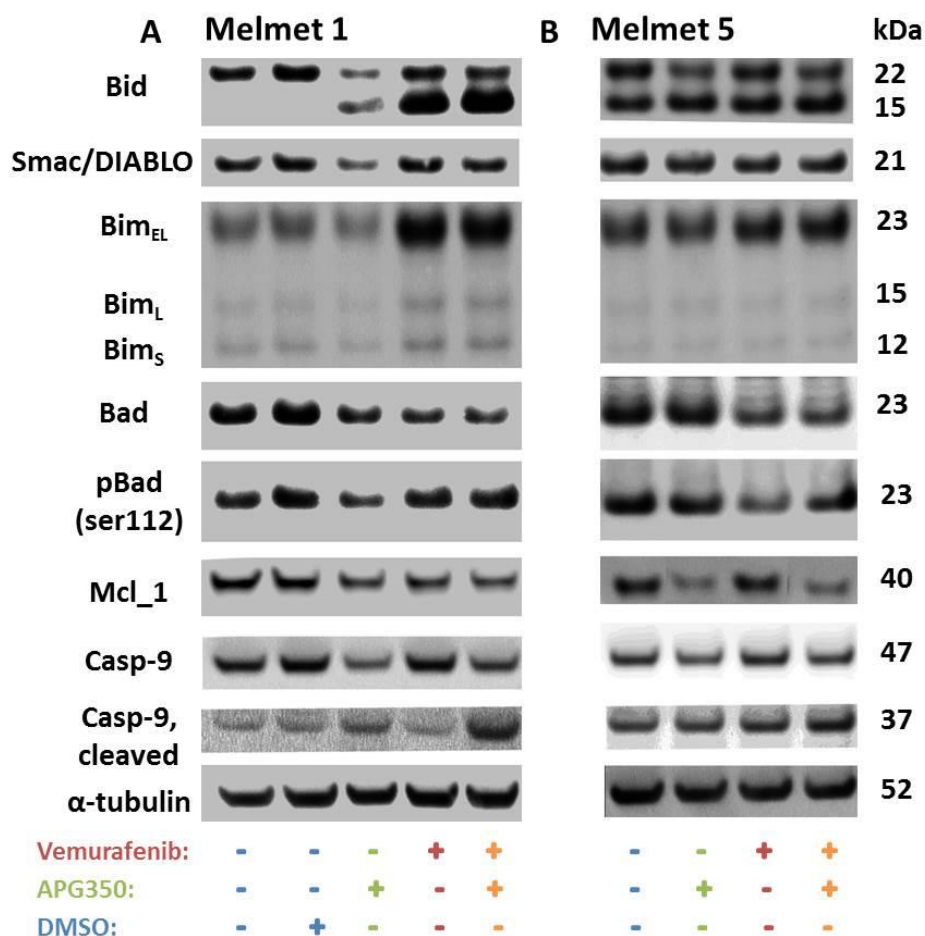


Figure 3.7: Western blots showing protein expression of intrinsic family members in Melmet 1 (A) and Melmet 5 (B). The blots presented are representative for three different biological experiments, except for Bid and Smac/DIABLO which were only performed once. DMSO controls were not included for the Melmet 5 cells in the shown parallel, but were included in the other parallels. The APG350 concentration = 0,1 µg/mL and vemurafenib concentrations = 0,33 µM.

Cleavage of Bid links the extrinsic and intrinsic pathway. In Melmet 1 (figure 3.7 A), Bid is cleaved in all therapies, but to a higher degree in samples treated with vemurafenib mono-therapy and combination therapy than in APG350 mono-therapy treated samples. In Melmet 5 (figure 3.7 B) the control sample displays cleaved Bid and there does not seem to be any substantial difference between control sample and the therapy treated samples. Smac/DIABLO, which is a pro-apoptotic protein, does not show any significant difference between control samples and therapy treated samples in Melmet 5, while Bim_{EL} is slightly increased in the combination therapy sample compared to the control sample. In Melmet 1, Smac/DIABLO is down-regulated only in APG350 treated samples. Bim is upregulated in samples treated with vemurafenib mono-therapy and combination therapy and APG350 mono-therapy samples are reduced. The pro-apoptotic protein Bad, on the other hand, is in both cell lines reduced in vemurafenib mono-therapy samples and combination therapy samples compared to control cells.

Phosphorylation of Bad inactivates the proteins pro-apoptotic abilities. In this study antibodies detecting pBad phosphorylated at serine 112 and 136 were investigated, both showing similar expression patterns (serine 112 is shown in figure 3.7). In Melmet 1, pBad expression is increased in both vemurafenib mono-therapy treated samples and combination therapy samples compared to the untreated control sample. Mcl-1, on the other hand, is reduced in the same samples. For APG350 treated samples, both proteins are reduced compared to the control samples. It should be noted that the DMSO control of the pBad-blot is increased compared to the untreated control. In Melmet 5, pBad is reduced in vemurafenib mono-therapy treated samples compared to the other samples. Mcl-1 is increased in the same sample when comparing to the other therapy treated samples, but similarly expressed as the control sample. Samples treated with APG350 mono-therapy and combination therapy are reduced in Mcl-1 compared to the control sample.

Caspase-9 is a caspase cleaved in the apoptosome and which can activate caspase-3. In Melmet 1, combination therapy induces more abundant cleavage of caspase-9 compared to control cells and mono-therapy treated samples. Caspase-9 in the APG350 treated samples is also cleaved, but less than in the samples treated with combination therapy. In Melmet 5, the same trends can be observed, but the differences are not as clear.

The protein pERK was analyzed to investigate the effect of vemurafenib on the cell lines. No effect on pERK was observed in any of the two cell lines after 24 hours (figure 3.8).

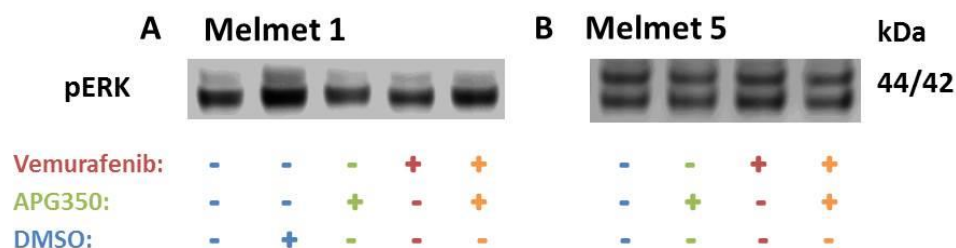


Figure 3.8: Western blots of the protein pERK in Melmet 1 (A) and Melmet 5 (B). The blot was executed from one biological experiment.

3.3 Evaluation of lung fibroblasts impact on Melmet cells exposed to vemurafenib and APG350

Stromal cells have been shown to have an impact on drug response³². To determine the impact lung fibroblasts have on vemurafenib- and APG350 therapy, either by secreted factors or by direct cell-cell

interactions, Melmet cells were cultured in conditioned medium from WI-38 lung fibroblasts or co-cultured with the WI-38 cells.

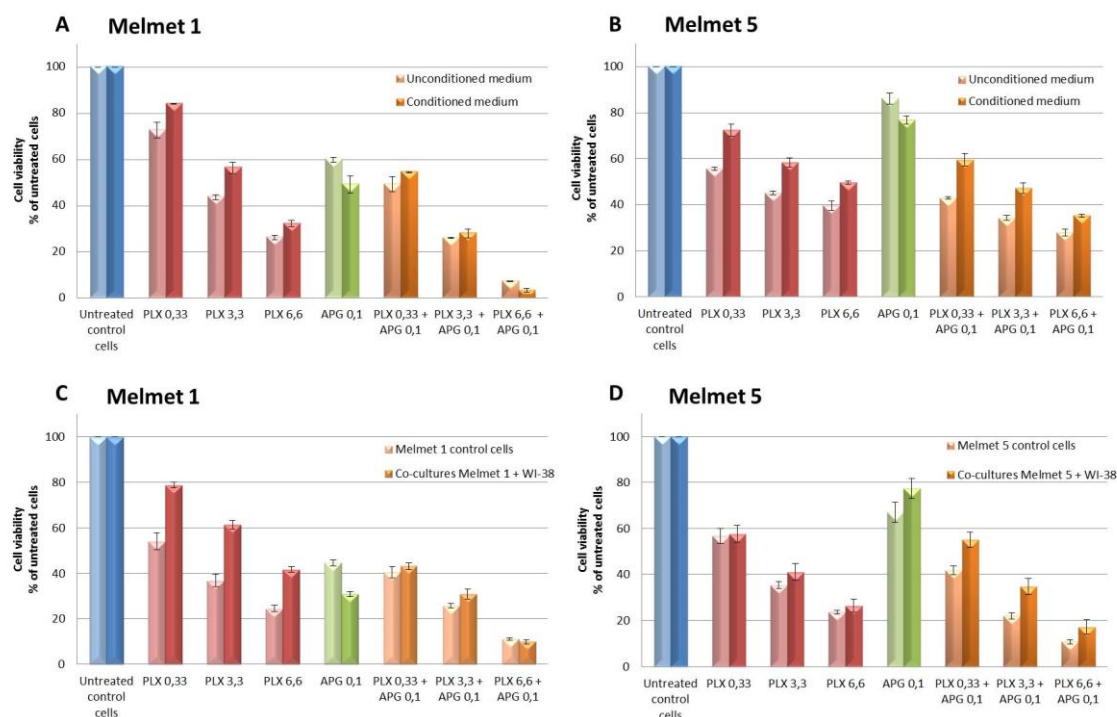


Figure 3.9: Melmet 1 (A&C) and Melmet 5 (B&D) cultured in conditioned medium from WI-38 fibroblasts (A&B) or as co-cultures with WI-38 fibroblast (C&D). Cells cultured in conditioned medium or as co-cultures are visualized as dark colored columns. Light colored columns are cells grown in normal, unconditioned medium or as mono-cultures consisting of Melmet cells. Concentrations of APG350 (APG) and/or vemurafenib (PLX) are indicated on the x-axis. Each column represents the average of three individual biological experiments showing the cell viability in % of untreated cells. Standard error of the mean (SEM) is indicated. 7000 cells/well were cultured for the conditioned medium experiments, 4000 cells per well were utilized in the co-culture experiments.

A difference in drug response is seen in both Melmet 1 and Melmet 5 when cells are cultured in conditioned medium (dark colored columns) vs. cells cultured with normal medium (light colored columns) (Figure 3.9 A and B). The effect of vemurafenib mono-therapy (red bars) is notably decreased in conditioned medium grown cells, indicating a rescue effect induced by factors in the conditioned medium. In APG350-treated cells (green bars), the conditioned medium interestingly inflicts an opposite effect; an increased dose response to the drug. For combination therapy the results differ between the cell lines. Melmet 1 does not get an obvious rescue effect from the conditioned medium, while Melmet 5 cells do. This is interesting as both cell lines show a similar response in mono-therapy.

In the co-culture experiments (figure 3.9 C and D), the fibroblast effects observed in Melmet 1 differ from the effects seen in Melmet 5 in all therapies. Melmet 1 is saved from vemurafenib mono-therapy

but not from combination therapy, and an increased dose response is seen in cells treated with APG350 mono-therapy. Melmet 5 cells, on the other hand, are rescued from combination therapy and APG350 mono-therapy, but not from vemurafenib mono-therapy. Comparing these results to the conditioned medium experiments (figure 3.9 A and 3.9 B) show consistency in the Melmet 1 cell line but differences in Melmet 5, though combination therapy shows the same rescue effect in both experiment types. It should be noted that the highest combination therapy doses of the microenvironment experiments seem to induce synergistic effects in Melmet 1 cells, unlike the initial 2D-culture experiments (figure 3.3 A).

3.4 Evaluation of mono-therapy and combination therapy in mouse lung tissue

The PuMA assay demonstrates the therapeutic response of vemurafenib and APG350 in Melmet 5 cells growing in a lung microenvironment with various stromal cells and ECM components. The photographs of the lung tissue sections (figure 3.10) indicate reduced growth of cancer cells in the tissue sections exposed to either mono-therapy or combination therapy compared to untreated control samples. In the control sections, the number of Melmet 5 colonies decreases in number but increases in size and intensity during the time period of the study. Mono-therapy of vemurafenib and APG350 inhibits colony growth both in size and number compared to the control cells, the effect of APG350 mono-therapy seemingly better than the effect of vemurafenib mono-therapy at the selected doses. Response to combination therapy seems better than the mono-therapies, even though the difference is less clear when comparing with APG350 mono-therapy. Substantial variation in regard to background fluorescence was observed for the different tissue sections.

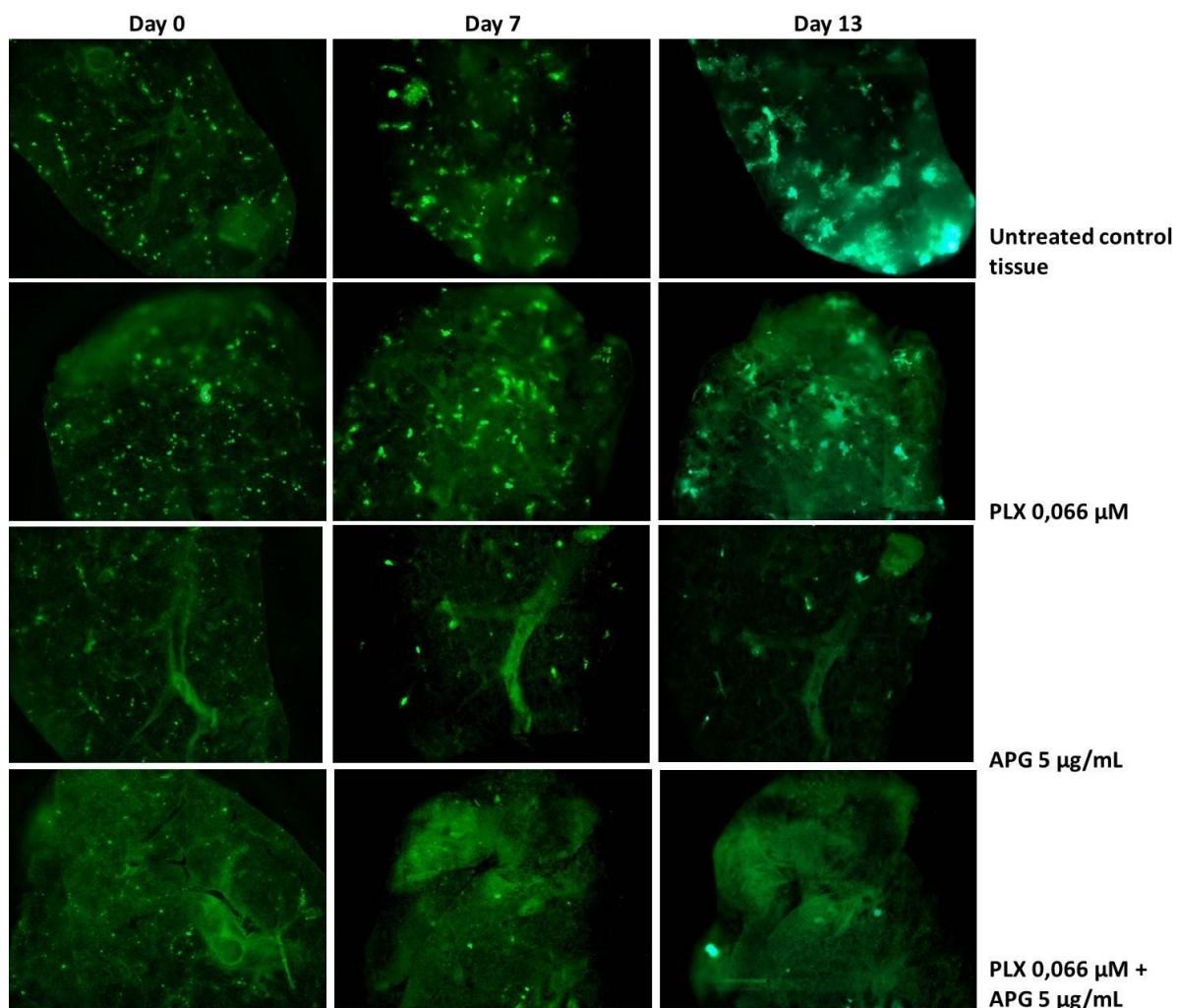


Figure 3.10: Fluorescent photographs of mouse lung tissue sections with Melmet 5 GFP-tagged cells. Selected treatment days and selected concentrations of APG350 (APG) and vemurafenib (PLX) are shown. Background fluorescence has been subtracted in the photographs to better visualize the colonies.

Quantification of intensity as integrated pixel density (mean grey value*area) was performed to get a more objective evaluation of the PuMA photographs. The results show that the Melmet 5 colonies have a relatively better response to combination therapy than to mono-therapy in the shown doses (figure 3.11), but that the standard deviations are very high, making the results unreliable. Note that APG350 as mono-therapy for the most part shows a higher intensity than vemurafenib as mono-therapy, something that differs from the photographs presented in figure 3.10.

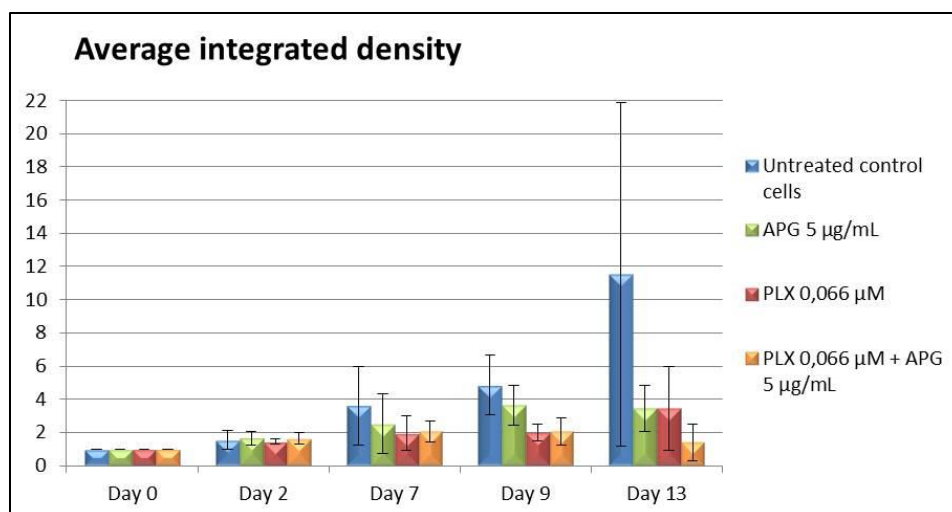


Figure 3.11: Average integrated density quantified from pictures of the PuMA tissue sections. The columns are presented relative to day 0. Two different areas of two parallel tissue sections (total of four areas) were analyzed by measuring integrated density using the ImageJ computer program. This value reflects the fluorescence intensity in the selected ROI. Standard deviation is shown. APG350 (APG) and vemurafenib (PLX) as mono-therapy are highlighted in green and red, respectively. Combination therapy is highlighted in orange.

Tissue sections were sent to immunohistochemistry staining after 13 days of culturing. The expression of GFP and KI-67 was monitored and are shown in figure 3.12. A clear difference in GFP- and KI-67-expression is observed when comparing the control tissue to the drug treated tissue, though APG350 mono-therapy and combination therapy are similar.

In addition to the concentrations presented in figure 3.10, 3.11 and 3.12, an APG350 dose of 1 µg/mL was included in the experiments. There was both a visual and a quantifiable reduction between 1 µg/mL and 5 µg/mL. See appendix Xd for the integrated density graphs containing all tested concentrations.

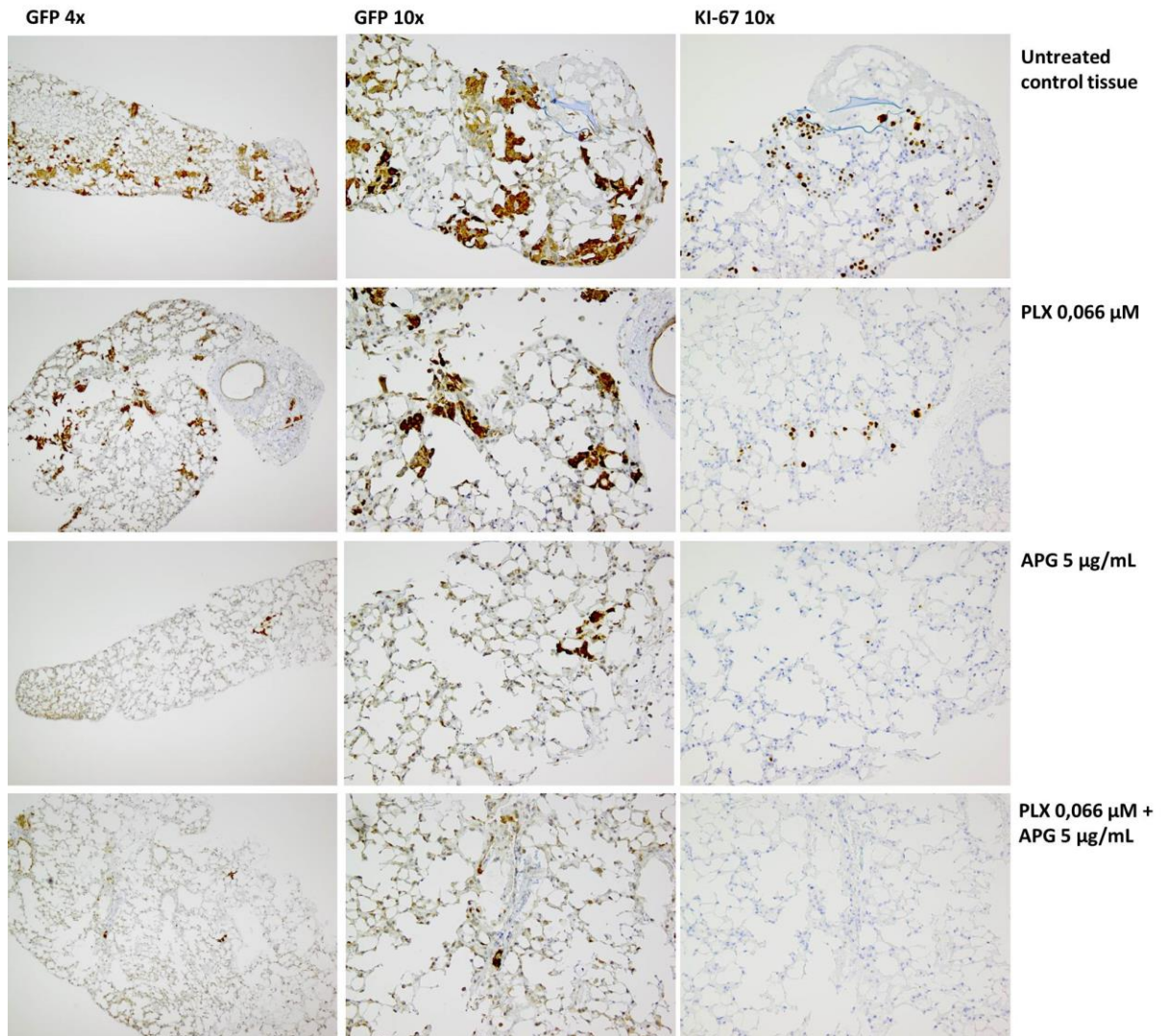


Figure 3.12: Expression of GFP and KI-67 in IHC stained tissue sections treated with APG350 (APG) and/or vemurafenib (PLX) vs. control medium for 13 days.

4. Discussion

In the present work, combination therapy with vemurafenib and APG350 has been evaluated in the cell lines Melmet 1 and Melmet 5, both with and without influence of microenvironmental factors. The cell lines are responsive to both drugs, and combination therapy leads to both synergistic and antagonistic effects depending on the cell line, culture type and drug dose utilized. Additionally, microenvironment factors affect the cancer cells response to therapy.

In Melmet 5, which is a proliferative, low invasive cell line, the 2D-culture experiments show that combinations of vemurafenib with APG350 doses above 0,01 $\mu\text{g}/\text{mL}$ induces synergistic effects compared to mono-therapy. This trend was confirmed in spheroids analyzed with the Glo-assay and in cells grown in lung tissue (results presented in chapter 3.1.3 and chapter 3.4). The Melmet 5 spheroid growth curves (figure 3.4 B), based on measurement of cell volume from day to day, did not indicate synergism. This may be explained by inaccuracy in the measurement of the spheroids. The Melmet 5 spheroids were more difficult to measure than Melmet 1 due to their edges being less defined when treated with combination therapy compared to untreated spheroids. Additionally, the density of the spheroids seemed to be reduced in response to therapy, making the perimeter blurred and the spheroids bigger.

Western analysis of the cell line shows that the extrinsic apoptosis pathway is activated to a higher degree in cells treated with combination therapy than mono-therapy, with more cleavage of caspase-3 and PARP. Active caspase-3 cleaves vital proteins in the cell, and the cleavage of PARP indicates that caspase-3 is functional. Protein members of the intrinsic apoptosis pathway were more ambiguously expressed, with the pro-apoptotic proteins Bad and Smac/DIABLO being both down-regulated and similarly expressed in combination therapy samples vs. control samples, and the anti-apoptotic protein pBad showing slight down-regulation. Bim is known to be a potent apoptosis inducer⁴³ and Bim_{EL} is slightly upregulated in the cell line. This, along with the downregulation of the anti-apoptotic protein Mcl-1 indicates that apoptosis through the intrinsic pathway is activated. Additionally, cleaved caspase-9 is to some extent increased in combination therapy treated samples. It is the balance between the pro- and anti-apoptotic proteins that determines to which degree apoptosis is initiated, and the limited range of proteins tested in this project is not sufficient to evaluate the pathways full activation status. If both the intrinsic and extrinsic apoptosis pathways are active, the cells will have a stronger apoptotic response than the extrinsic pathway alone. Overall, the results give a strong indication that the Melmet 5 cell line responds better to combination therapy compared to vemurafenib mono-therapy, the standard treatment offered to V600E mutated BRAF patients to date.

Melmet 1, which is an invasive, low proliferative cell line, shows varying response to combination therapy depending on the culturing method and drug dose utilized. In 3D-cultures, the spheroids clearly show an additional effect of combination therapy compared to mono-therapy when considering both the growth curves (figure 3.4 A) and Glo-results (figure 3.5 A). In the 2D-cultures, on the other hand, combination therapy does not give synergistic effects in the cells. Quite the contrary, many of the tested drug doses lead to an increase in cell survival, indicating that combination of the two drugs may induce cancer-favorable responses in the cells. Interestingly, Western analysis of Melmet 1 cells cultured in 2D indicate higher apoptosis activation in combination therapy vs. mono-therapy treated cells, as seen in the levels of cleaved caspase-8, cleaved caspase-3 and cleaved PARP (figure 3.6). Additionally, the cleavage of Bid and caspase-9 indicates that also the intrinsic apoptosis pathway is active, and the upregulation of all Bim variants and downregulation of Mcl-1 support this claim. All data indicates activation of apoptosis and increased cell death in combination therapy contrary to the 2D-cell viability results. This suggests that resistance mechanisms downstream of the proteins investigated in this study may be active, or that caspase-3 is partly inhibited e.g. by XIAP. It should be noted that cells for Western analysis were harvested 24 hours after treatment while cell viability assays were performed 72 hours after treatment and the results are therefore not directly comparable. Some proteins are likely to be differently expressed at the two time points and cells for Western analysis should therefore have been harvested at several different time points.

There exists convincing evidence that 3D-cultures are better mimics of living tissue and more accurately reflects complex *in vivo* environments compared to cells grown as 2D-monolayers^{31, 34, 66, 67}. Therapy response in cells may thus differ depending on the culture type utilized^{68, 69}. Based on these studies and the promising 3D results for Melmet 1, it is possible that Melmet 1 will be sensitive to combination therapy *in vivo*.

It should be noted that Melmet 1 does not form spheroids spontaneously as Melmet 5 does. They are dependent on Matrigel for spheroid-formation, and it was not determined if the Matrigel affects the cells' therapy response. However, the microscope photographs of the spheroids (figure 3.4 C and D) show that Melmet 1 differs from Melmet 5 in appearance, seeming looser and less dense. One can speculate if the anatomy of the Melmet 1 spheroids may help the drugs penetrate into the spheroid and in that way better distribute its effect, leading to increased therapy response. If this is the case it may explain why Melmet 1 is more sensitive to vemurafenib than Melmet 5 in 3D-cultures, when opposite results are observed in the 2D-cultures.

As mentioned in Results chapter 3.3, Melmet 1 cells show a beneficial effect of combination therapy in the microenvironment experiments, unlike what was observed in the initial 2D-culture experiments. Some of the experimental factors differ between the experiments, which may explain the observed

variation. Firstly, the MTS-, Glo- and luciferase-assays were utilized interchangeably, but when compared it was shown that similar results were obtained regardless of assay used (data not shown). The number of Melmet cells was reduced in co-cultures to make room for fibroblast cells, and a low cell number increased the effect of vemurafenib and APG350, as seen when comparing drug response in co-cultures (figure 3.9 C and D) to response in conditioned medium experiments (figure 3.9 A and B). This was also evaluated in a separate experiment where 4000 vs. 7000 Melmet cells per well was compared (data not shown). One can speculate if the increased cell death occurs because the drugs have a better effect on fewer cells or if they are less content when they have fewer neighbors of similar cell type and therefore die more easily. In addition to this, the vemurafenib concentration was increased in TME-experiments to evaluate if higher vemurafenib doses would give increased effect of combination therapy in Melmet 1. The two highest doses do induce an additional effect in combination therapy treated cells vs. mono-therapy treated cells, but the results also show that all the tested doses of vemurafenib mono-therapy are more potent than what was observed in the initial 2D-combination therapy experiments. Whether this increased vemurafenib effect is due to differences between the utilized vemurafenib batches or something else is not known. In any case, these results indicate that increased vemurafenib doses may counteract antagonistic effects observed from the initial 2D-combination therapy.

Explanations of the antagonism seen in 2D-cultures of Melmet 1 when combining the two drugs can be related to studies of pro-survival mechanisms induced by TRAIL. TRAIL has been related to ERK activation^{49, 70, 71}, NF- κ B activation⁴⁸, as well as activation of the PI3K-AKT-pathway⁷⁰. Studies show that TRAIL-induced ERK activation is associated with suppression of apoptosis⁷⁰ and Zhang et. al. (2003)⁷¹ has provided evidence that TRAIL-mediated ERK activation protects melanoma cell lines from apoptosis by inhibiting Smac/DIABLO release from the mitochondria. In this study the Smac/DIABLO expression (figure 3.7) was decreased after 24 hours only in APG350 treated samples and not in combination therapy, and pERK expression remained unchanged after exposure to all therapies (figure 3.8). However, the localization of Smac/DIABLO was not studied and may still be mitochondrial. The lack of pERK inhibition after vemurafenib treatment was unexpected since both cell lines show response to vemurafenib in cell viability assays. This could be related to the harvesting time point or the vemurafenib concentration utilized. It should also be noted that the results of pERK, Smac/DIABLO and Bid expression were only studied in cells from one biological experiment.

Another TRAIL-induced survival mechanism is related to the activation of AKT, which can lead to phosphorylation of Bad at serine 136⁷². Bad is a pro-apoptotic protein which when phosphorylated will be sequestered and left inactive, thereby suppressing cell death. The expression of pBad is however not increased after APG350-treatment in this study, indicating that AKT in this case is not activated by TRAIL. AKT can also activate IKK, a subunit of NF- κ B, leading to activation of the NF- κ B

transcription factor. Protein products downstream of NF- κ B have not been investigated here, but TRAIL-resistant cells have been shown to activate NF- κ B leading to increased proliferation⁴⁸. The cells of this study are not fully resistant as they show a dose dependent response to low APG350 concentrations, but because higher doses do not give additional effects it may imply that innate resistance is an issue.

Resistance to vemurafenib after initial response is well-documented, and several resistance mechanisms are identified^{23,24}. High levels of activated NRAS and increased levels of C-Raf are often found in cell lines with acquired vemurafenib resistance and may lead to reactivation of the MAPK-pathway. Indirect activation of PI3K-AKT is also a proposed resistance mechanism. Combination therapy is a much used strategy to overcome resistance. When combining vemurafenib with APG350 one not only targets the MAPK-pathway but also activates apoptotic pathways. In theory, targeting several cellular pathways simultaneously could shift the cells balance toward death, hopefully overcoming resistance issues. But it is also possible that the combination provides over-stimulation of other survival pathways, like PI3K-AKT which in theory is activated by both vemurafenib and APG350. To summarize, the two drugs have the potential to activate different cellular pathways which can interact with each other to shift the cells balance in favor of survival or death. It can be hypothesized that combination therapy in some cases may shift the cells balance toward survival, explaining the antagonism seen in 2D-cultures of Melmet 1. Even when combination therapy induces synergy, these alternative pathways may contribute to reduce the effect of combination therapy on the cells. Additional studies are needed to identify mechanisms involved when combining the two drugs.

Vemurafenib is dissolved in DMSO, and in our hands DMSO alone increased the cell viability of both cell lines by up to 30 % in 2D-cultures (figure 3.2) and up to 10 % in spheroids (figure 3.5). The increase in cell viability has been observed by other representatives in Gunhild Mælandsmo's group, but is not directly documented in the literature. However, DMSO's ability to induce cell differentiation and cell-surface alterations has previously been shown⁷³⁻⁷⁵, and Bentel et. al. (1990)⁷⁶ reported that epithelial cell lines cultured in the presence of DMSO could lead to enhanced invasiveness. Additionally, DMSO's protective effects in different models have been previously reported, as reviewed by Kelava et.al. in 2011⁷⁷. These data suggests that DMSO possesses properties that can affect the cells, and thereby DMSO present in the vemurafenib solution may influence drug response, making the dose response curves skewed. By relating the dose responses to DMSO control cells instead of untreated control cells the data may be more representable. Graphs showing this are included in the appendix Xe. Oddly, DMSO does not seem to increase cell survival in vemurafenib mono-therapy treated cells, as seen by the lack of increase in the blue graph in figure 3.3 A. Why this is the case is not known, but it may seem that DMSO alone and in combination with the two tested drugs has an adverse effect on cells which is not triggered by vemurafenib alone.

The effect of the tumor microenvironment (TME) on tumor response to therapy has been previously documented in several articles^{32, 68, 78-80}, where Straussman et al. (2012)³² show that several fibroblast cell lines, WI-38 included, can induce melanoma cell resistance to RAF-inhibitors. In the present study, WI-38 lung fibroblasts decrease the effect of vemurafenib and increase the effect of APG350. In Melmet 1 the fibroblasts do not seem to affect combination therapy, while a rescue effect is seen in combination therapy of Melmet 5. The conditioned medium experiments indicate that it is fibroblast secreted factors which contribute to rescue the Melmets from therapy. For instance Hepatocyte growth factor (HGF) secreted by fibroblast cells can reactivate the MAPK pathway, PI3K-AKT-pathway and the HGF receptor MET in melanoma cells, thereby contributing to RAF-inhibitor resistance³². Cell-cell contact, as simulated by the co-culture experiments, was comparable to conditioned medium results in Melmet 1. In Melmet 5, however, cell-cell contact may counteract the protecting effects of fibroblast-secreted factors on mono-therapy treated cells, while combination therapy remained unchanged. It must be emphasized that different cell-types present in the TME may affect tumor cells in several ways, and that the TME experiments of this study only indicate the effect of WI-38 fibroblasts. In the PuMA-assay, on the other hand, a wider variety of TME-factors are present and the results of the assay reveal that the tested drugs induce toxic effects on Melmet 5 growing in a lung environment. It can therefore be assumed that factors of the TME in this case are not able to save the cancer cells from therapy. However, it is not known whether the drugs' effects are reduced due to TME-interactions.

It should be noted that the PuMA-assay, developed by Mendoza et al.⁶⁵, is a new and not fully established assay at the Department of Tumor Biology. Experiences and knowledge acquired during this project have contributed to a more optimized protocol, but the data presented in this thesis is not standardized to the extent that is required for publications and the assay was only performed once. The standard error calculated for the average integrated density data are very high (figure 3.11), reflecting a large variation between the tissue sections and areas analyzed. This variation is probably due to two major factors. Firstly, the ROI being analyzed in each photograph was placed manually and the tissue morphology to some extent changed each time the sections were turned, making the exact same placement of the ROI difficult. Secondly, and probably even more critical, is the fact that the number of colonies in each tissue section on day 0 showed substantial variation, as well as different growth patterns during the extent of the experiment. Colony growth in some cases seemed to be directed "downwards" below the tissue surface, while in other cases the growth was lateral in the surface area. This will give variations in regard to the fluorescence intensity detected that does not relate to the actual colony growth or size. By utilizing a tissue slicing machine which can provide more evenly and thinner slices of tissue than manual slicing, it might be possible to diminish this variation to a more acceptable level. Additionally it has been proposed that by using the IncuCyte™ live content imaging system (Essen BioScience), the exact same part of each tissue section will be photographed each day.

Additionally, the IncuCyte™ may solve issues in regard to varying picture quality and background fluorescence.

In summary, the present project has shown that combination therapy with APG350 and vemurafenib is capable of reducing growth of Melmet cells in several culture types and that the tumor microenvironment does affect the therapy efficacy. Differences between the cell lines were shown, with Melmet 5 giving more consistent results than Melmet 1. These variations may reflect upon the cell lines differences in phenotype, stressing the importance of a thorough examination and profiling of patient material before initiation of therapy. Importantly, results of the present project emphasize that TME-interactions need to be taken into account when designing new therapy regimens.

Future perspectives

The relative short time period of this project causes several questions to be left unanswered, and further investigations are necessary before any conclusions about the effect of vemurafenib and APG350 in combination can be drawn.

First of all, to confirm the results of the present project, more melanoma cell lines need to be tested to validate the generality of the drug combinations. Additionally, different factors of the experiments need to be more strictly controlled; therefore additional studies on the influence of Matrigel on therapy response should be initiated, along with further studies of how to reduce DMSO's effect on melanoma cells. Cell lines which are resistant to vemurafenib and cells resistant to TRAIL-treatment ought to be tested to evaluate if combination therapy can help overcome resistance. The effect of combination therapy on stromal cells should also be tested.

Resistance mechanisms activated by combination therapy, potentially leading to increased cell survival, need to be explored to a greater extent. Proteins part of the NF κ B and PI3K-AKT signal pathways, as well as proteins related to caspase-3 inhibition, like IAPs and cFLIP, should be investigated. Additional studies of Smac/DIABLO and ERK-activation is also necessary.

The PuMA-assay needs further optimization by implementing the proposed changes of utilizing a slicing machine for preparation of lung sections and using the IncuCyte™ for live imaging. If these alterations prove successful the assay should be utilized on several melanoma cell lines. This can give interesting information regarding melanoma cells response to combination therapy in an environment to which they tend to metastasize. An important step would also be to test the effect of combination therapy *in vivo* in mouse-models.

References

1. Webpage. (2012). *Melanoma* [Encyclopedia]. In Zieve, D. & Eltz, D. R. (eds): MedlinePlus. Available at: <http://www.nlm.nih.gov/medlineplus/ency/article/000850.htm> (accessed: 19th february 2013).
2. Report. (2012). Cancer in Norway 2010 - Cancer incidence, mortality, survival and prevalence in Norway. In Larsen, I. K. (ed.). Oslo: Cancer Registry of Norway.
3. Uong, A. & Zon, L. I. (2010). Melanocytes in development and cancer. *Journal of Cellular Physiology*, 222 (1): 38-41.
4. Tuong, W., Cheng, L. S. & Armstrong, A. W. (2012). Melanoma: Epidemiology, Diagnosis, Treatment, and Outcomes. *Dermatologic Clinics*, 30 (1): 113-124.
5. Gilchrist, B. A., Eller, M. S., Geller, A. C. & Yaar, M. (1999). The pathogenesis of melanoma induced by ultraviolet radiation. *N Engl J Med*, 340 (17): 1341-8.
6. Miller, A. J. & Mihm, M. C. (2006). Melanoma. *New England Journal of Medicine*, 355 (1): 51-65.
7. Armstrong, B. K. & Krickler, A. (2001). The epidemiology of UV induced skin cancer. *J Photochem Photobiol B*, 63 (1-3): 8-18.
8. Webpage. *Melanoma statistics and outlook*: Cancer Research UK. Available at: <http://www.cancerresearchuk.org/cancer-help/type/melanoma/treatment/melanoma-statistics-and-outlook#meloverall> (accessed: 19th february 2013).
9. Kudchadkar, R., Paraiso, K. H. & Smalley, K. S. (2012). Targeting mutant BRAF in melanoma: current status and future development of combination therapy strategies. *Cancer J*, 18 (2): 124-31.
10. Wan, P. T. C., Garnett, M. J., Roe, S. M., Lee, S., Niculescu-Duvaz, D., Good, V. M., Project, C. G., Jones, C. M., Marshall, C. J., Springer, C. J., et al. (2004). Mechanism of Activation of the RAF-ERK Signaling Pathway by Oncogenic Mutations of B-RAF. *Cell*, 116 (6): 855-867.
11. Poulikakos, P. I., Persaud, Y., Janakiraman, M., Kong, X., Ng, C., Moriceau, G., Shi, H., Atefi, M., Titz, B., Gabay, M. T., et al. (2011). RAF inhibitor resistance is mediated by dimerization of aberrantly spliced BRAF(V600E). *Nature*, 480 (7377): 387-90.
12. Weber, C. K., Slupsky, J. R., Kalmes, H. A. & Rapp, U. R. (2001). Active Ras induces heterodimerization of cRaf and BRaf. *Cancer Res*, 61 (9): 3595-8.
13. Montagut, C. & Settleman, J. (2009). Targeting the RAF-MEK-ERK pathway in cancer therapy. *Cancer Lett*, 283 (2): 125-34.
14. Bollag, G., Hirth, P., Tsai, J., Zhang, J., Ibrahim, P. N., Cho, H., Spevak, W., Zhang, C., Zhang, Y., Habets, G., et al. (2010). Clinical efficacy of a RAF inhibitor needs broad target blockade in BRAF-mutant melanoma. *Nature*, 467 (7315): 596-9.
15. Davies, H., Bignell, G. R., Cox, C., Stephens, P., Edkins, S., Clegg, S., Teague, J., Woffendin, H., Garnett, M. J., Bottomley, W., et al. (2002). Mutations of the BRAF gene in human cancer. *Nature*, 417 (6892): 949-954.
16. Wang, Y. F., Jiang, C. C., Kiejda, K. A., Gillespie, S., Zhang, X. D. & Hersey, P. (2007). Apoptosis induction in human melanoma cells by inhibition of MEK is caspase-independent and mediated by the Bcl-2 family members PUMA, Bim, and Mcl-1. *Clin Cancer Res*, 13 (16): 4934-42.
17. Finn, L., Markovic, S. & Joseph, R. (2012). Therapy for metastatic melanoma: the past, present, and future. *BMC Medicine*, 10 (1): 23.

18. Flaherty, K. T., Puzanov, I., Kim, K. B., Ribas, A., McArthur, G. A., Sosman, J. A., O'Dwyer, P. J., Lee, R. J., Grippo, J. F., Nolop, K., et al. (2010). Inhibition of mutated, activated BRAF in metastatic melanoma. *N Engl J Med*, 363 (9): 809-19.
19. Bhatia, S., Tykodi, S. S. & Thompson, J. A. (2009). Treatment of metastatic melanoma: an overview. *Oncology (Williston Park)*, 23 (6): 488-96.
20. Patrawala, S. & Puzanov, I. (2012). Vemurafenib (RG67204, PLX4032): a potent, selective BRAF kinase inhibitor. *Future Oncol*, 8 (5): 509-23.
21. Rubinstein, J. C., Sznol, M., Pavlick, A. C., Ariyan, S., Cheng, E., Bacchiocchi, A., Kluger, H. M., Narayan, D. & Halaban, R. (2010). Incidence of the V600K mutation among melanoma patients with BRAF mutations, and potential therapeutic response to the specific BRAF inhibitor PLX4032. *J Transl Med*, 8: 67.
22. Klinac, D., Gray, E. S., Millward, M. & Ziman, M. (2013). Advances in personalized targeted treatment of metastatic melanoma and non-invasive tumor monitoring. *Front Oncol*, 3: 54.
23. Su, F., Bradley, W. D., Wang, Q., Yang, H., Xu, L., Higgins, B., Kolinsky, K., Packman, K., Kim, M. J., Trunzer, K., et al. (2012). Resistance to selective BRAF inhibition can be mediated by modest upstream pathway activation. *Cancer Res*, 72 (4): 969-78.
24. Shi, H., Moriceau, G., Kong, X., Lee, M. K., Lee, H., Koya, R. C., Ng, C., Chodon, T., Scolyer, R. A., Dahlman, K. B., et al. (2012). Melanoma whole-exome sequencing identifies (V600E)B-RAF amplification-mediated acquired B-RAF inhibitor resistance. *Nat Commun*, 3: 724.
25. Das Thakur, M., Salangsang, F., Landman, A. S., Sellers, W. R., Pryer, N. K., Levesque, M. P., Dummer, R., McMahon, M. & Stuart, D. D. (2013). Modelling vemurafenib resistance in melanoma reveals a strategy to forestall drug resistance. *Nature*, 494 (7436): 251-5.
26. Poulikakos, P. I., Zhang, C., Bollag, G., Shokat, K. M. & Rosen, N. (2010). RAF inhibitors transactivate RAF dimers and ERK signalling in cells with wild-type BRAF. *Nature*, 464 (7287): 427-30.
27. Paget, S. (1989). The distribution of secondary growths in cancer of the breast. 1889. *Cancer Metastasis Rev*, 8 (2): 98-101.
28. Steeg, P. S. (2003). Metastasis suppressors alter the signal transduction of cancer cells. *Nat Rev Cancer*, 3 (1): 55-63.
29. Alberts, B., Johnson, A., Lewis, J., Raff, M., Roberts, K. & Walter, P. (2008). The Tumor Microenvironment Influences Cancer Development. In Anderson, M. & Granum, S. (eds) *Molecular Biology of the Cell*, pp. 1222-1223. United States of America: Garland Science.
30. Joyce, J. A. & Pollard, J. W. (2009). Microenvironmental regulation of metastasis. *Nat Rev Cancer*, 9 (4): 239-52.
31. Abbott, A. (2003). Cell culture: biology's new dimension. *Nature*, 424 (6951): 870-2.
32. Straussman, R., Morikawa, T., Shee, K., Barzily-Rokni, M., Qian, Z. R., Du, J., Davis, A., Mongare, M. M., Gould, J., Frederick, D. T., et al. (2012). Tumour micro-environment elicits innate resistance to RAF inhibitors through HGF secretion. *Nature*, 487 (7408): 500-4.
33. Vinci, M., Gowan, S., Boxall, F., Patterson, L., Zimmermann, M., Court, W., Lomas, C., Mendiola, M., Hardisson, D. & Eccles, S. A. (2012). Advances in establishment and analysis of three-dimensional tumor spheroid-based functional assays for target validation and drug evaluation. *BMC Biol*, 10: 29.
34. Pampaloni, F., Reynaud, E. G. & Stelzer, E. H. (2007). The third dimension bridges the gap between cell culture and live tissue. *Nat Rev Mol Cell Biol*, 8 (10): 839-45.
35. Wong, R. (2011). Apoptosis in cancer: from pathogenesis to treatment. *Journal of Experimental & Clinical Cancer Research*, 30 (1): 87.

36. Alberts, B., Johnson, A., Lewis, J., Raff, M., Roberts, K. & Walter, P. (2008). Apoptosis. In Anderson, M. & Granum, S. (eds) *Molecular Biology of the Cell*, pp. 1115-1128. United States of America: Garland Science.
37. Duprez, L., Wirawan, E., Vanden Berghe, T. & Vandenabeele, P. (2009). Major cell death pathways at a glance. *Microbes Infect*, 11 (13): 1050-62.
38. Cotter, T. G. (2009). Apoptosis and cancer: the genesis of a research field. *Nat Rev Cancer*, 9 (7): 501-7.
39. O'Brien, M. A. & Kirby, R. (2008). Apoptosis: A review of pro-apoptotic and anti-apoptotic pathways and dysregulation in disease. *Journal of Veterinary Emergency and Critical Care*, 18 (6): 572-585.
40. Hao, Z. & Mak, T. W. (2010). Type I and type II pathways of Fas-mediated apoptosis are differentially controlled by XIAP. *J Mol Cell Biol*, 2 (2): 63-4.
41. Eckelman, B. P., Salvesen, G. S. & Scott, F. L. (2006). Human inhibitor of apoptosis proteins: why XIAP is the black sheep of the family. *EMBO Rep*, 7 (10): 988-94.
42. Zhang, N., Hartig, H., Dzhagalov, I., Draper, D. & He, Y. W. (2005). The role of apoptosis in the development and function of T lymphocytes. *Cell Res*, 15 (10): 749-69.
43. Jiang, C. C., Lai, F., Tay, K. H., Croft, A., Rizos, H., Becker, T. M., Yang, F., Liu, H., Thorne, R. F., Hersey, P., et al. (2010). Apoptosis of human melanoma cells induced by inhibition of B-RAFV600E involves preferential splicing of bimS. *Cell Death Dis*, 1: e69.
44. Shih, M. *Regulation of BAD phosphorylation* [Webpage]. BioCarta, Pathways. Available at: http://www.biocarta.com/pathfiles/h_badpathway.asp (accessed: April 3rd).
45. Dimberg, L. Y., Anderson, C. K., Camidge, R., Behbakht, K., Thorburn, A. & Ford, H. L. (2012). On the TRAIL to successful cancer therapy? Predicting and counteracting resistance against TRAIL-based therapeutics. *Oncogene*.
46. Nagane, M., Huang, H. J. & Cavenee, W. K. (2001). The potential of TRAIL for cancer chemotherapy. *Apoptosis*, 6 (3): 191-7.
47. Thorburn, A., Behbakht, K. & Ford, H. (2008). TRAIL receptor-targeted therapeutics: resistance mechanisms and strategies to avoid them. *Drug Resist Updat*, 11 (1-2): 17-24.
48. Ehrhardt, H., Fulda, S., Schmid, I., Hiscott, J., Debatin, K. M. & Jeremias, I. (2003). TRAIL induced survival and proliferation in cancer cells resistant towards TRAIL-induced apoptosis mediated by NF-kappaB. *Oncogene*, 22 (25): 3842-52.
49. Zhang, X. D., Zhang, X. Y., Gray, C. P., Nguyen, T. & Hersey, P. (2001). Tumor necrosis factor-related apoptosis-inducing ligand-induced apoptosis of human melanoma is regulated by smac/DIABLO release from mitochondria. *Cancer Res*, 61 (19): 7339-48.
50. Schulze-Osthoff, K., Ferrari, D., Los, M., Wesselborg, S. & Peter, M. E. (1998). Apoptosis signaling by death receptors. *European Journal of Biochemistry*, 254 (3): 439-459.
51. Gura, T. (1997). How TRAIL kills cancer cells, but not normal cells. *Science*, 277 (5327): 768.
52. Gieffers, C., Kluge, M., Meinolf, T., Merz, C., Sykora, J., Fischer, C., Branschädel, M., Fricke, H. & Hill, O. (2012). *Dimerized single chain TRAIL-receptor agonist do not depend on FC-gamma-receptor cross-linking for anti-tumor efficacy in vivo*. 103rd Annual Meeting of the American Association for Cancer Research, Chicago, IL: Cancer Research.
53. Maiuri, M. C., Zalckvar, E., Kimchi, A. & Kroemer, G. (2007). Self-eating and self-killing: crosstalk between autophagy and apoptosis. *Nat Rev Mol Cell Biol*, 8 (9): 741-52.
54. Fink, S. L. & Cookson, B. T. (2006). Caspase-1-dependent pore formation during pyroptosis leads to osmotic lysis of infected host macrophages. *Cell Microbiol*, 8 (11): 1812-25.
55. Hellenes, T. (2009). *Mapping the expression of anti-apoptotic proteins and evaluation of the therapeutic potential of TRAIL receptor antibodies in "close-to-patient" melanoma models*. Department of Tumor Biology, Institute for Cancer Research, The Norwegian Radium

- Hospital, Oslo University Hospital: University of Oslo, Department of Molecular Biosciences, Faculty of Mathematics and Natural Sciences. 93 pp.
56. Prasmickaite, L., Engesaeter, B. O., Skrbo, N., Hellenes, T., Kristian, A., Oliver, N. K., Suo, Z. & Maelandsmo, G. M. (2010). Aldehyde dehydrogenase (ALDH) activity does not select for cells with enhanced aggressive properties in malignant melanoma. *PLoS One*, 5 (5): e10731.
 57. Day, C. P., Carter, J., Bonomi, C., Esposito, D., Crise, B., Ortiz-Conde, B., Hollingshead, M. & Merlino, G. (2009). Lentivirus-mediated bifunctional cell labeling for in vivo melanoma study. *Pigment Cell Melanoma Res*, 22 (3): 283-95.
 58. Protocol. (2012). *CellTiter 96 Aqueous One Solution Cell Proliferation Assay*. TB245. USA: Promega Corporation.
 59. Crouch, S. P., Kozlowski, R., Slater, K. J. & Fletcher, J. (1993). The use of ATP bioluminescence as a measure of cell proliferation and cytotoxicity. *J Immunol Methods*, 160 (1): 81-8.
 60. Protocol. (2012). *CellTiter-Glo Luminescent Cell Viability Assay*. TB288. USA: Promega Corporation.
 61. Webpage. (2013). *Overview of Western Blotting*: Thermo Scientific. Available at: <http://www.piercenet.com/browse.cfm?fldID=8259A7B6-7DA6-41CF-9D55-AA6C14F31193> (accessed: March 1st, 2013).
 62. Protocol. (2011). *Pierce BCA Protein Assay Kit*. USA: Thermo Fisher Scientific Inc.
 63. Diller, T. M., J., Updyke, T., Feldman, G., Simcha, I. & Szafranski, C. *A New Dry Blotting System for Rapid Protein Transfer for Polyacrylamide Gels to Membranes*. Invitrogen (ed.).
 64. Webpage. (2013). *iBlot 7-minute Blotting System*. USA: Life technologies. Available at: http://www.invitrogen.com/site/us/en/home/Products-and-Services/Applications/Protein-Expression-and-Analysis/Western-Blotting/Western-Blot-Transfer/iBlot-Dry-Blotting-System.html?s_kwcid=TC|17958|iblot||S|p|12437420286 (accessed: March 1st).
 65. Mendoza, A., Hong, S.-H., Osborne, T., Khan, M. A., Campbell, K., Briggs, J., Eleswarapu, A., Buquo, L., Ren, L., Hewitt, S. M., et al. (2010). Modeling metastasis biology and therapy in real time in the mouse lung. *The Journal of Clinical Investigation*, 120 (8): 2979-2988.
 66. Griffith, L. G. & Swartz, M. A. (2006). Capturing complex 3D tissue physiology in vitro. *Nat Rev Mol Cell Biol*, 7 (3): 211-24.
 67. Ghosh, S., Spagnoli, G. C., Martin, I., Ploegert, S., Demougin, P., Heberer, M. & Reschner, A. (2005). Three-dimensional culture of melanoma cells profoundly affects gene expression profile: a high density oligonucleotide array study. *J Cell Physiol*, 204 (2): 522-31.
 68. McMillin, D. W., Delmore, J., Weisberg, E., Negri, J. M., Geer, D. C., Klippel, S., Mitsiades, N., Schlossman, R. L., Munshi, N. C., Kung, A. L., et al. (2010). Tumor cell-specific bioluminescence platform to identify stroma-induced changes to anticancer drug activity. *Nat Med*, 16 (4): 483-9.
 69. Grigorieva, I., Thomas, X. & Epstein, J. (1998). The bone marrow stromal environment is a major factor in myeloma cell resistance to dexamethasone. *Exp Hematol*, 26 (7): 597-603.
 70. Falschlehner, C., Emmerich, C. H., Gerlach, B. & Walczak, H. (2007). TRAIL signalling: decisions between life and death. *Int J Biochem Cell Biol*, 39 (7-8): 1462-75.
 71. Zhang, X. D., Borrow, J. M., Zhang, X. Y., Nguyen, T. & Hersey, P. (2003). Activation of ERK1/2 protects melanoma cells from TRAIL-induced apoptosis by inhibiting Smac/DIABLO release from mitochondria. *Oncogene*, 22 (19): 2869-81.
 72. Datta, S. R., Dudek, H., Tao, X., Masters, S., Fu, H., Gotoh, Y. & Greenberg, M. E. (1997). Akt phosphorylation of BAD couples survival signals to the cell-intrinsic death machinery. *Cell*, 91 (2): 231-241.

73. Joshi, S. S., Jackson, J. D. & Sharp, J. G. (1985). Differentiation inducing effects of butyrate and DMSO on human intestinal tumor cell lines in culture. *Cancer Detect Prev*, 8 (1-2): 237-45.
74. Dairkee, S. H. & Glaser, D. A. (1982). Dimethyl sulfoxide affects colony morphology on agar and alters distribution of glycosaminoglycans and fibronectin. *Proc Natl Acad Sci U S A*, 79 (22): 6927-31.
75. Jiang, G., Bi, K., Tang, T., Wang, J., Zhang, Y., Zhang, W., Ren, H., Bai, H. & Wang, Y. (2006). Down-regulation of TRRAP-dependent hTERT and TRRAP-independent CAD activation by Myc/Max contributes to the differentiation of HL60 cells after exposure to DMSO. *Int Immunopharmacol*, 6 (7): 1204-13.
76. Bentel, J. M., Rhodes, G. C., Markus, I. & Smith, G. J. (1990). Enhanced invasiveness and metastatic potential of epithelial cell lines cultured in the presence of dimethyl sulphoxide. *Int J Cancer*, 46 (2): 251-7.
77. Kelava, T., Cavar, I. & Culo, F. (2011). Biological actions of drug solvents. *Periodicum Biologorum*, 113 (3): 311-320.
78. Shekhar, M. P., Santner, S., Carolin, K. A. & Tait, L. (2007). Direct involvement of breast tumor fibroblasts in the modulation of tamoxifen sensitivity. *Am J Pathol*, 170 (5): 1546-60.
79. Wang, W., Li, Q., Yamada, T., Matsumoto, K., Matsumoto, I., Oda, M., Watanabe, G., Kayano, Y., Nishioka, Y., Sone, S., et al. (2009). Crosstalk to stromal fibroblasts induces resistance of lung cancer to epidermal growth factor receptor tyrosine kinase inhibitors. *Clin Cancer Res*, 15 (21): 6630-8.
80. Kim, S. J., Kim, J. S., Park, E. S., Lee, J. S., Lin, Q., Langley, R. R., Maya, M., He, J., Kim, S. W., Weihua, Z., et al. (2011). Astrocytes upregulate survival genes in tumor cells and induce protection from chemotherapy. *Neoplasia*, 13 (3): 286-98.

Appendix

I) List of reagents and materials

Reagents and materials:	Company:	Cat. #:
1 M Tris		
5 M NaCl		
10 M NaOH		
12 M HCl		
20 % Tween		
APG350	Apogenix	
BX51 system microscope	Olympus	
BX-UCB, external system controller	Olympus	
Cell scraper 30 cm	TPP®	99003
CellTiter 96® Aqueous One Solution Reagent	Promega	G3580 G3581
CellTiter-Glo® Reagent	Promega	G7571
CKX41 inverted microscope	Olympus	
Corning® 96 Well Flat Clear Bottom White Polystyrene TC-Treated Microplate	Corning Incorporated	3610
Corning® 96 Well Flat Clear Bottom Black Plate, TC-treated	Corning Incorporated	3603
Corning® 96 Well Clear Round Bottom Ultra Low Attachment Microplate	Corning Incorporated	7007
Countess™-automated cell counter	Invitrogen™	C10227
Countess™-cell counting chamber slides	Invitrogen™	C10283
D-Luciferin 1g	BioThema	BT11-1000
Dimethyl Sulphoxide (DMSO) Hybri-max™	Sigma-Aldrich	D2650
EDTA Versene® 0,02 %	Lonza, BioWhittaker®	BE17-711E
Eagle's Minimum Essential Medium (EMEM)	ATCC	30-2003
Finnpipette® Stepper pipette	Thermo Scientific	4540
Finntip® Stepper tips	Thermo Scientific	9404
Fetal calf serum (FCS)	PAA	A15-101
Formalin, 4 %	Merck	
Gelfoam® 12-7mm absorbable, 12cm ²	Pfizer	272575
GlutaMAX™ (100x)	Gibco® by Life technologies	35050-038

Appendix

Glycine	Merck	
Huvec super, MVDB 131 medium (1x)	Gibco® by Life technologies	10372-019
iBlot Gel Transfer Stacks Nitrogencellulose, regular	Invitrogen™	IB3010-01
iBlot™ blotting machine	Invitrogen™	
IX81® Motorized Inverted Microscope	Olympus	
IX2-UCB external system controller	Olympus	
Matrigel™ Basement Membrane Matrix	BD Biosciences	354234
NuPAGE® Novex 4-12 % Bis-Tris Midi Gel	Invitrogen™	WG1401BOX
NuPAGE® LDS sample buffer (4x)	Invitrogen™	NP0008
NuPAGE® MES SDS Running Buffer (20x)	Invitrogen™	NP000202
NuPAGE® Sample reducing agent (10x)	Invitrogen™	NP0009
Nunc™ EasYflasks, nunclon delta treated with blue filter cap.	Thermo Scientific	156499 156367
Nunclon Delta Surface, 96-well plate	Thermo Scientific	167008
Nunclon Delta Surface, 24-well plate	Thermo Scientific	142475
PBS	BioWhittaker®	BE17-516F
PowerEase™500	Invitrogen™	
M199 medium (1x)	Gibco® by Life technologies	31150-022
Phosphatase inhibitor cocktail tablets, PhosSTOP	Roche	04 906 837 001
Pierce® Bovine Serum Albumin Standards	Thermo Scientific	23209
Pierce® BCA Protein Assay Kit	Thermo Scientific	23227
Pierce® BCA Protein Assay Reagent A	Thermo Scientific	23228
Pierce® BCA Protein Assay Reagent B	Thermo Scientific	23224
Protease inhibitor cocktail tablets, cOmplete Mini	Roche	04 693 124 001
RPMI 1640 cell medium	BioWhittaker®	BE12-167F
SeeBlue® Plus2 Prestained Standard (1x)	Invitrogen™	LC5925
SuperSignal® West Dura Extended Duration Substrate	Thermo Scientific	# 34076
SuperSignal® West Dura Stable Peroxide Buffer	Thermo Scientific	#1859025
SuperSignal® West Dura Luminol/Enhancer Solution	Thermo Scientific	# 1859024
Syringe, 10 mL	BD Plastipak™	302188
Syringe filter, 0,45 µm cellulose acetate	VWR	28145-481
Trypan Blue stain 0,4 %	Gibco® by Life techonlogies	15250-061
UltraPure™ 1M Tris-HCl, pH 7.5	Invitrogen™	15567-027

Vemurafenib/PLX 4032	Selleck Chemicals LLC	S1267 Batch: S126703 S126705 S126709
Wallac Victor ² 1420 Multilabel counter	Wallac	
X-Cite® 120 PC Q, fluorescence light source	Lumen Dynamics	

II) Details related to the Calcusyn data program

The CI value of non-exclusive treatments is calculated by the formula:

$$CI = (Da + Db)/(Dxa + Dxb) + Da*Db/Dxa*Dxb.$$

Da and Db are doses needed of treatment A and B to inhibit x % of cell proliferation as single treatments, and Dxa and Dxb are the doses of A and B to inhibit x % of cell growth in a combination regimen.

III) Example of spheroid volume calculations

The volume inside a sphere is derived to be $V = \frac{4}{3}\pi r^3$ where r is the radius of the sphere. If Cell[^]P measured the mean radius of the spheroid to be 418,14 μm the volume will be 306231894,5 μm^3 equivalent to 0,306 mm^3 .

IV) Luciferin solution

1. D-Luciferin 1 g (BioThema) was dissolved in 35 mL PBS to make a white solution with approximately pH 5.
2. Use 10M NaOH to adjust the pH to 7,5 – 7,8.
3. If pH is too high, adjust with HCl
4. Fill to 50 mL with PBS.
5. Store at -20°C.

V) Lysis buffer

For 50 mL lysis buffer:

20 mM Tris-HCl pH 7,5	= 1 mL 1M Tris-HCL pH 7,5
137 mM NaCl	= 1,37 mL 5 M NaCl
100 mM NaF	= 5 mL 1 M Na F
10 % Glycerol	= 5 mL Glycerol
1 % NP-40	= 5 mL 10 % NP-40
	Fill with dH ₂ O to 50 mL

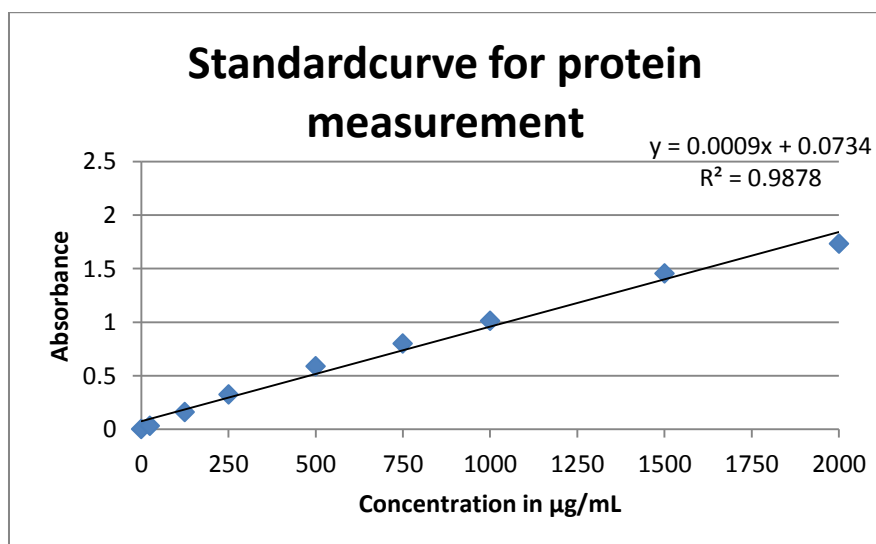
Add 1 protease inhibitor cocktail tablet, cOmplete Mini (Roche) to 500 μ L dH₂O.

Add 1 phosphatase inhibitor cocktail tablet, PhosSTOP (Roche) to 500 μ L dH₂O.

50 μ L phosphatase stop and 50 μ L protease stop is added to 1 mL lysis buffer.

VI) Example of protein concentration and protein volume calculations

The Pierce BCA Protein Assay Kit (Thermo Scientific) was utilized to measure the absorbance of each sample in two parallels. The average of the parallels was calculated and the background absorbance subtracted. The protein concentration was calculated utilizing the standard curve equation (see example below), where x = concentration and y = absorbance. Note that the concentrations calculated are for diluted samples and needs to be converted.



Example of protein concentration calculation:

The sample absorbance minus background absorbance = 0,220.

$$x = \frac{(0,220 - 0,0734)}{0,0009}$$

$$x = 163,06 \mu\text{g}/\text{mL}$$

Since the samples were diluted (5 μL sample + 55 μL lysisbuffer), the concentration of undiluted sample needed to be calculated using the formula below:

$C1 \cdot V1 = C2 \cdot V2$

C1= Concentration of undiluted sample
 V1= Volume of undiluted sample = 5 μL
 C2= Concentration of diluted sample
 V2= End volume after dilution = 60 μL

$$C1 = \frac{163,06 \mu\text{g}/\text{mL} * 60 \mu\text{L}}{5 \mu\text{L}}$$

$$C1 = 1956,7 \mu\text{g}/\text{mL}$$

10 μg of sample was to be applied on the gel. Calculation of volume was done with the formula below where V = volume, m = mass and c = concentration:

$$V = \frac{m [\mu\text{g}]}{c [\mu\text{g}/\text{mL}]}$$

$$V = \frac{10 \mu\text{g}}{1956,7 \mu\text{g}/\text{mL}}$$

$$V = 0,00511 \text{ mL} = 5,11 \mu\text{L}$$

The volume of sample to be applied to the gel (5,11 μL) was diluted with lysis buffer to a total volume of 10 μL .

VII) R&D-buffer, pH 7,5

For 1 L R&D-buffer:

25 mM Tris pH 7,5 = 25 mL 1M Tris
0,15M NaCl = 30 mL 5M NaCl
0,1 % Tween = 5 mL 20 % Tween
Fill with dH₂O to 1 L

VIII) Stripping solution

For 1 L Stripping solution:

7,5 g Glycine
900 mL dH₂O
10 mL 12M HCl pH 2,2 (=37 %)
Fill with dH₂O to 1 L

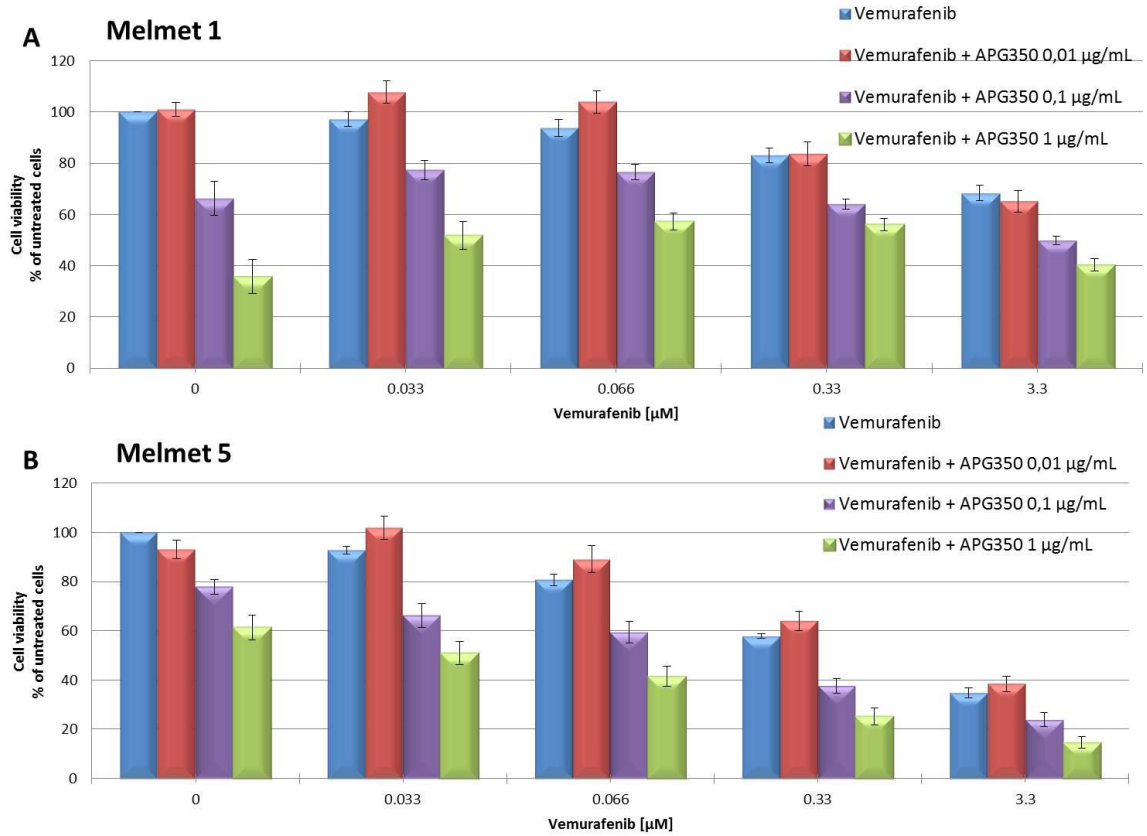
IX) PuMA-medium

1x) Medium M199 (1x)
 Crystalline bovine insulin – 1 µg/mL
 Hydrocortisone – 0,1 µg/mL
 Retinyl acetate – 0.1 µg/mL
 Penicillin/Streptomycin – 10 µl/mL

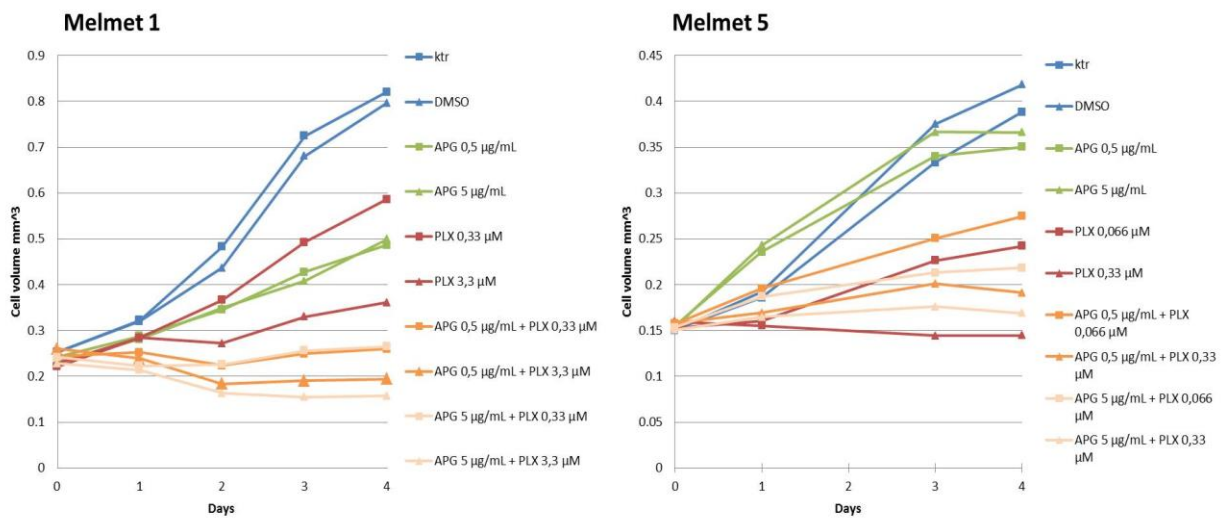
2x) Medium M199 (2x)
 Crystalline bovine insulin – 2 µg/mL
 Hydrocortisone – 0,2 µg/mL
 Retinyl acetate – 0.2 µg/mL
 Penicillin/Streptomycin – 20 µl/mL

X) Supplementary data

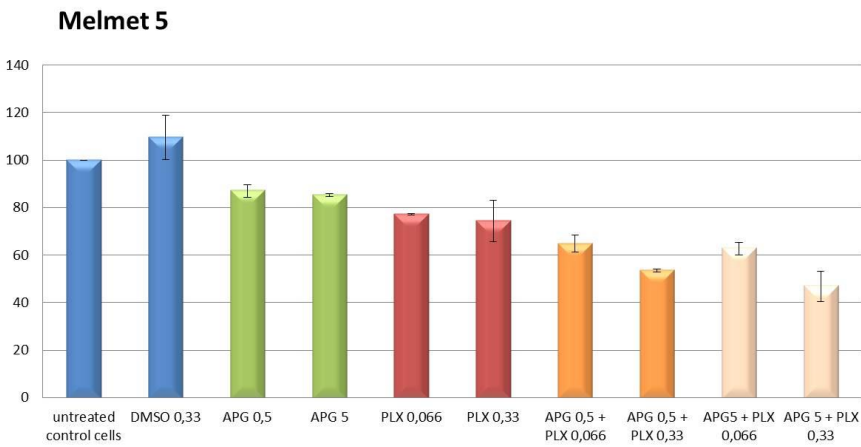
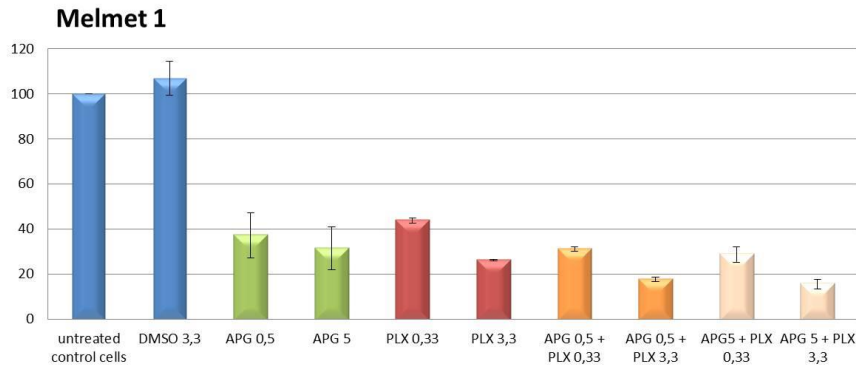
a) Combination therapy graphs presented as column charts



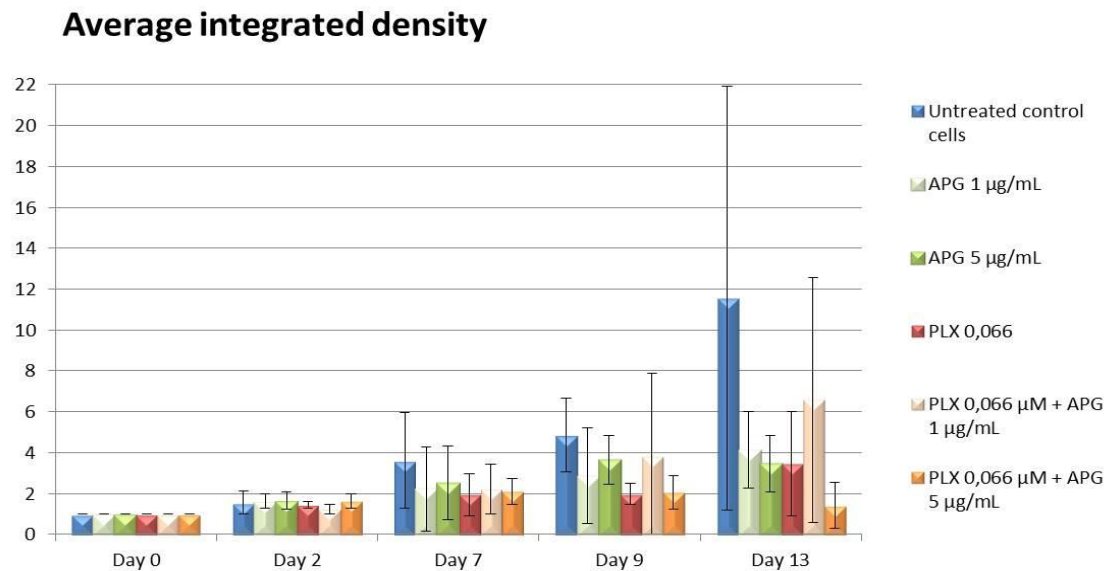
b) Spheroid growth curves of all tested drug concentrations



c) Glo-graphs of all tested drug concentrations



d) PuMA-quantification graphs including all tested drug concentrations



e) Combination therapy graphs related to DMSO-control cells

